INTERNAL DOCUMENT

No. 177

A Field Study Evaluation of the triple axis Coherent Doppler Velocity Profiler for measuring near-bed flow

K. F. E. Betteridge, P. S. Bell,
P. D. Thorne and J. J. Williams

December 2005

www.pol.ac.uk

Proudman Oceanographic Laboratory
NATURAL ENVIRONMENT RESEARCH COUNCIL

A Field Study Evaluation of the triple axis Coherent Doppler Velocity Profiler for measuring near-bed flow:

K.F.E. Betteridge, P.S. Bell, P.D. Thorne, and J.J. Williams

Proudman Oceanographic Laboratory, Joseph Proudman building,
6 Brownlow Street, Liverpool. L3 5DA, UK.

Abstract

Existing commercially available triple axis profiling instruments do not provide co-located velocity measurements which are important for studying sediment transport processes. A triple axis Coherent Doppler Velocity Profiler, CDVP, has been developed at POL to improve our capability to make co-located triple axis profiling measurements. It was tested at sea during the INDIA multi-disciplinary field study and the data was used to assess if near-bed turbulent and intra-wave flow could be measured over a 1 m depth above the sea bed.

The CDVP was designed to measure orthogonal velocity profiles within a narrow column of water at 16 Hz, within 1 m of the bed, with a vertical spatial resolution of 0.05 m. This report describes the first deployment of the instrument, in a tidal inlet in Portugal, and a comparison of the CDVP flow velocity measurements with data from other instrumentation. An assessment was made against two commercially available Acoustic Doppler Velocimeters, ADVs. Measurements of the mean and fluctuating velocity profiles were collected with the triple axis CDVP and the results showed reasonable agreement with measurements obtained with the ADVs at frequencies up to 4 Hz, with a difference occurring above the noise floor of the CDVP.

Contents

1. Introduction

Instruments to study near-bed sediment transport processes are under continual development in order to advance scientific understanding of sediment entrainment, hydrodynamics and bedform evolution. In particular, to examine the details of sediment entrainment, it is necessary to measure intra-wave and near-bed turbulence. Acoustic instrumentation continues to be developed because such measurements are largely non-intrusive, provide profiles with centimetric spatial resolution and resolve turbulent time scales, Thorne and Hanes, 2002, Zedel and Hay, 1999.

Instruments which contribute to these measurements include the following, but they also have limitations;

1) Acoustic Doppler velocimeters, ADV's, provide a significant contribution to high resolution measurements, but they are limited to three component observations at one location in the water column. (Voulgaris and Trowbridge, 1998).

2)Uni-axial coherent Doppler velocity profilers, CDVP's measure the radial component of the turbulent flow field over a range of up to 1.5 m with a resolution of the order of centimetres (Hardcastle, 1994, Zedel et al, 1996, Zedel and Hay, 1999, Veron and Melville 1999, Thorne and Taylor, 2000, Betteridge et al, 2002). In these systems fluid velocities are determined from the rate of change of phase of consecutive acoustic signals backscattered from suspended sediments. The axial component of the flow profile may therefore be obtained; however, these systems have been limited to measuring the flow in a single direction.

3) The commercially available Sontek Coherent Doppler Profiler measures profiles of orthogonal turbulent flow components (see www.sontek.com). This instrument can provide 2 Hz three axis velocity profiles in centimetric range cells. However, the system uses diverging beams and therefore does not provide co-located velocity profiles. This can be a serious shortcoming in many hydrodynamic and sediment processes studies.

To overcome these limitations, triple-axis CDVPs are being developed to obtain co-located measurements of the three orthogonal components of flow. There is literature on the development and use of such technology in laboratory tests for marine applications e.g. Hurther and Lemmin 1998, Hurther and Lemmin, 2001, Rolland and Lemmin, 1997, Zedel and Hay, 2002, Wilson et al, 2000. This report describes the development and results from the first reported marine trial of a triple axis CDVP developed using converging beams, and is a summary of a paper (Betteridge et al, in press 2005) with an expansion of the results to include all records from one day of the deployment

considered. The CDVP was deployed during the European funded field study INDIA, where other proven current measuring instrumentation was used and advantage was taken of this study to assess the development of the CDVP within a marine setting. The deployment was on the POL Instrument Package at the entrance to a tidal lagoon at Ria Formsa, Algarve, Portugal during the multi-disciplinary INDIA study (Williams, 2003a), and the instruments in the project were located on an instrument package deployed on a jack-up barge (Williams et al, 2003b). There was a wave-current environment at the tidal inlet site, with strong currents measuring from 0.4-2 ms^{-1} and waves with significant height, H_s, of around 0.75 m and period, T_p, of about 5 s; the sea bed was composed of coarse sand.

The CDVP consisted of one transceiver and two passive receivers. These were configured to measure profiles of the three orthogonal components of the flow. Initially the mean, time averaged, velocities measured by the CDVP were compared with the mean velocities measured by the two ADVs and the outcome gave very comparable results. This was followed by detailed comparisons of the 16 Hz measurements of the flow by both the CDVP and ADV; time series, power spectra, statistics and regression analysis were used to quantify the capability of the CDVP. The results show very comparable velocity measurements, although there are some differences associated with a spatial separation between the ADVs and CDVP measurement volumes and some shortcomings in the CDVP itself.

.

2. Instrument design - Coherent Doppler Systems

(a)Coherent Doppler processing

Measurements of the vertical profile of the backscattered signal were obtained within closely spaced range bins by range gating. The radial velocity was obtained from the rate of change of the phase of consecutive backscattered signals (Zedel et al,1996 and Veron and Melville, 1999). The phase Ψ is given by

$$\Psi = \tan^{-1}\left(\frac{\langle I(t)Q(t+T) - I(t+T)Q(t)\rangle}{\langle Q(t)Q(t+T) + I(t)I(t+T)\rangle}\right) \quad (1)$$

where T is the delay between transmission pulses, I(t) and Q(t) are the in-phase and quadrature components of the received signal and <> represents an average over a number of consecutive pulse pairs. The Doppler frequency shift f_d is given by

$$f_d = \frac{\Psi}{2\pi T} \quad (2)$$

and the radial velocity v_d by

$$v_d = \frac{cf_d}{2f_0} \quad (3)$$

where c is the sound velocity in water and f_o is the transmit frequency. The return from the i^{th} pulse at the maximum range must be received before pulse (i+1) is transmitted to obtain unambiguous range information. The rate of pulse transmission, the pulse repetition frequency, PRF, determines the maximum unaliased value of the Doppler frequency f_d and the maximum range-velocity relationship is given by $r_m v_{dm} \leq c^2/8f_0$ where r_m is the maximum range and v_{dm} is the maximum unaliased velocity that may be measured.

An early version of the CDVP used a PRF, of 512 Hz which gave an unambiguous velocity range given by $V_{\max} = \frac{PRF * c / f_0}{4}$ of ±0.36 m s^{-1} based on a Doppler phase shift of $\pm\pi$ with c=1500m/s and f_0=524kHz; for the flow velocities greater than this, the Doppler phase shift signal aliased. Velocities in excess of this are frequently experienced in oceanographic environments, therefore to overcome this limitation the triple axis CDVP employed a dual PRF approach (Lhermitte & Serafin, 1984). Applying this technique, the present system used two interleaved PRFs of 512Hz and 409.6Hz with a timing ratio of 5/4 to further extend this unambiguous range, by

generating two Doppler shift frequencies, the combination of which provided a unique solution to the water velocity up to 4 times the unambiguous limit of the single 512Hz PRF, i.e. $\pm$ 1.46ms^{-1} in the radial direction of each transducer.

The coherent Doppler system produced complex phase information on the backscattered acoustic signal by mixing the returning signal with in-phase (I) and quadrature (Q) signals derived from the transmitter oscillator. The hardware to carry out this complex demodulation was of in-house design (Hardcastle, 1994), and the resulting I and Q components were sampled using a 16 bit PC based analogue to digital card sampling the I and Q signals simultaneously at 16384 Hz. The resulting phase information contained in the components of the complex signal was used in a four quadrant arctan algorithm to extract the Doppler phase shift as given by equation 1. The system was designed to produce velocity readings at 16Hz, allowing time for 28 pulses to be transmitted with interleaved PRFs, or 14 pulse pairs for each PRF at each time step. Equation 1 was applied to the data from each PRF separately, generating two related Doppler phase shifts for each sixteenth of a second sample. Assuming low noise data, the combination of these two Doppler phase shifts relates to a unique velocity up to the combined ambiguity limit of $\pm$1.46ms^{-1}. The two Doppler phase shifts for the two PRFs were logged by the PC recording software at 16Hz ready for de-aliasing.

The de-aliasing was realised in post-processing software by trying all possible aliasing combinations and choosing the combination and hence the velocity that yielded the lowest velocity difference between the Doppler shifts from the two PRFs. If the data were perfect and noiseless, one of these combinations would yield identical velocities. In reality there was noise on the signals, and so spike detection routines were also implemented to reduce instances of incorrect de-aliasing. This de-aliasing software was fully automatic, requiring no operator intervention. The resulting velocity values were further geometrically corrected to give orthogonal velocity components.

(b) Triple axis system application

The triple axis CDVP described here was designed to provide co-located vertical profiles of the three orthogonal components of the flow; u, the streamwise, v, crosswise, and w, vertical flow. The CDVP consisted of a vertically mounted, downward looking narrow beam disc transducer, Tz, which transmitted a short pulse. The backscattered signal was received on the downward looking transducer and also by two passive receivers located at 90 ° to each other in the horizontal plane. The beam patterns for the

two receiving transducers were specified for the purpose of receiving the backscattered signal from the whole vertical range insonified by the downward looking transducer (Betteridge et al, in press 2005). A diagram showing the CDVP transducer configuration is shown in figure 1. The vertical transducer, Tz, operated at 524 kHz, and had a -3 dB beam angle of approximately 1°. The two passive receivers, Rx and Ry were chosen to be resonant at 530 kHz and were located orthogonally to Tz in the same horizontal plane and at a distance of 0.585 m. They were rectangular transducers which received the sound signal with fan shaped beam patterns, with a -3dB full beam angle of 46° in the vertical, and a horizontal -3dB beam angle of 2.9°. Each transducer measured the radial velocity component derived from the backscattered sound as it propagated to the bed, thereby yielding co-located velocity profiles.

Referring to figure 1, the measured orthogonal flow velocities, u_m, v_m and w_m, were obtained from the de-aliased radial velocities V(Rx), V(Ry) and V(Tz) as follows. The velocity **V** is given by $\mathbf{V} = u_m\mathbf{i} + v_m\mathbf{j} + w_m\mathbf{k}$, where **i**, **j** and **k** are the unit vectors in the 3 orthogonal directions x, y and z. The transceiver, Tz, measures the vertical flow component, w_m, directly. Receiver Ry was measuring components of v_m and w_m, and the radial velocity measured by Ry, V(Ry), is given by;

$$V(Ry) = v_m \cos\theta_y + w_m \sin\theta_y \quad (5)$$

The crosswise flow velocity, v_m, may therefore be expressed as;

$$V_m = \tan\theta_y\,(V(Ry)/\sin\theta_y - V(Tz)) \quad (6)$$

where $V(Tz) = w_m$.

For the streamwise flow component, u, from Rx and Tz;

$$V(Rx) = -v_m \cos\theta_x + w_m \sin\theta_x \quad (7)$$

and therefore

$$u_m = \tan\theta_x\,(-\,(V(Rx)/\sin\theta_x + V(Tz)) \quad (8)$$

where the angles θ_x and θ_y were determined from the measurements of the distances between transducers and the acoustic travel time relating to each bin location.

The position of each velocity reading for this work was taken as the centre of the range cell. Small measurement inaccuracies in the positions of the transducers relative to each other could easily contribute to errors in the geometrical transformation at this stage and it would be preferable in future work to use a precision made jig to mount the transducers and eliminate such positioning uncertainty.

3. Experimental set-up and field site

The triple axis CDVP was deployed from a jack-up barge in a tidal inlet, in the Algarve, Portugal. Figure 2a shows the alignment of the jack-up barge to the current and wave directions and the X, Y, Z, co-ordinate system. The instruments were aligned into the tidal flow direction and the wave direction was at approximately 45 ° to the current flow, as shown by the arrows.

The CDVP instrument was attached to the PIP (POL Instrument Package) together with acoustic backscatter transducers, Acoustic Doppler Velocimeters (ADV's), electromagnetic current metres and pressure sensors (Williams et al, 2003b). The instrumented PIP is shown in the photograph in figure 2b, and the spacing between each transducer is listed in table 1. The notation ADV-N and ADV-S is used for the Nortek and Sontek ADVs respectively. The instrumentation frame was configured to have the main instrumentation and measuring volumes 0.5 m upstream from the main support frame, pointing into the combined wave-current flows to minimize interference to the flow measurements.

Table 1 Table shows the displacement in the three orthogonal directions between the ADV measurement volumes and the transmitting and receiving transducers of the triple axis CDVP, as shown in figure 5.

Measurement volume	X	Y	Z
ADV-S - Tz	0.525 m	0.185	0.80 m
ADV-S - Rx	0.060 m	0.185	0.77 m
ADV-S - Ry	0.525 m	0.475 m	0.75 m
ADV-N - Tz	0.405 m	0.185	0.70 m
ADV-N - Rx	0.180 m	0.185	0.67 m
ADV-N - Ry	0.405 m	0.475 m	0.65 m
ADV-N – ADV-S	0.12 m	0	0.10 m

The ADV instruments were located at approximately 0.15 m and 0.22 m above a flat bed and measured velocities at 25 Hz. The triple axis CDVP was located approximately 0.8 m above the bed and recorded velocity measurements at 16 Hz in 0.05 m range bins. Owing to the vertical beam width of the receiving transducers, the first receiver range bin with overlapping u, v and w measurements was at 0.66 m above the bed, and there

were 12 0.05m bins measuring below this down to the bed. Data from the Doppler profiler at the range bins coincident with the ADV measurement volumes were compared with the velocities measured by the two ADV's. The ADV's velocity measurements were used as a reference to assess the CDVP at its present stage of development. The acoustic instruments were spaced apart on the frame to minimize interference between them. Owing to the main flow being in the negative X direction, it was considered that the observed flow would only be marginally modified by the instrument package, Williams et al, 2003a, and any modifications to the flow that did occur would have the same impact on both the CDVP and ADV measurements.

As noted above, the instruments were aligned such that the X axes of the velocity measuring devices were directed into the main direction of the tidal flow. As shown in figure 2a, the convention taken was that the streamwise flow was denoted u, measured in the X-direction, with positive flow being taken as flow toward the instruments, ie in the negative X direction, the crosswise flow component was denoted v, in the Y direction and the vertical flow, w, in the Z direction. A diagram showing the relative locations of the triple axis CDVP and the 2 ADVs is shown in figure 3. Distances between each instrument are summarised in Table 1. It should be noted that there was a streamwise displacement of 0.405 m and 0.525 m between the measurement volumes of ADV-N and ADV-S respectively and the CDVP, and a displacement of 0.185 m between both ADV measurement volumes and the CDVP. This impacted on the coherence of the velocities recorded by the different instruments as discussed later.

The field site consisted of a mobile bed of coarse sand, mean diameter, d_{50}= 1.2 mm, with migrating bedforms of nominal heights and wavelength of 0.1 m and 1.0 m Pumped sample measurements showed that the suspended sediment size varied from about 200 μm to 500 μm and suspended sediment concentrations were between 0.005-0.5 kgm^{-3}. In order to test the capabilities of the triple axis CDVP, data obtained on 28 February 1999 were selected, when a set of records over a flood tide were available. Data collection spanned a period of 4 hours during the flood tide. On this day, $H_s \approx$ 0.75 m and $T_p \approx$5 s, the mean current speed varied from 0.4-2 ms^{-1} and the water depth from 2-3.5 m.

4. Results

To assess the capability of the profiling Doppler system in the field, a comparison of the results obtained with the triple axis CDVP and the two ADV's has been made. The velocity data from the CDVP and the ADV were corrected for misalignment relative to the main flow in the vertical and horizontal planes using a rotation matrix, $T = \begin{pmatrix} \cos\varphi & -\sin\varphi \\ \sin\varphi & \cos\varphi \end{pmatrix}$, where for a rotation about the z-axis, φ is the angle between the mean data and the x-axis. The velocities u_l and v_l of the rotated data were thus $\begin{pmatrix} u_l \\ v_l \end{pmatrix} = T\begin{pmatrix} u_m \\ v_m \end{pmatrix}$, where u_m and v_m are the measured velocities. Similarly $\begin{pmatrix} u \\ w_l \end{pmatrix} = T\begin{pmatrix} u_l \\ w_m \end{pmatrix}$ and $\begin{pmatrix} v \\ w \end{pmatrix} = T\begin{pmatrix} v_l \\ w_l \end{pmatrix}$. The data u, v, and w were the final rotated velocities for zero mean cross-flow and vertical flow. The measured and rotated data are plotted in figure 4, showing the angle, $\varphi = \tan^{-1}(\langle v \rangle / \langle u \rangle)$, where $\langle\rangle$ denotes the mean. The rotation was applied to each data set to obtain the flow parallel to the bed.

(i) Comparison of CDVP and ADV time-averaged velocity measurements

The triple axis CDVP recorded velocity measurements at 16 Hz, and the ADV instruments at 25 Hz, however, an initial comparison of the measurements was made using the measured mean velocity. The mean was obtained over the recording interval of 1024 s for the instruments, over a four hour flood period. The range bins of the CDVP closest to the ADVs were chosen for the comparison. These occurred at 0.07 m and 0.18 m above the average bed location for the ADV-S and ADV-N respectively. The mean velocities recorded for the 3 instruments are plotted over a flood cycle in figure 5. The error bar in the CDVP measurement is based on the difference in the velocities between two adjacent range bins, this being approximately equivalent to the difference in velocity which would be measured at the top and the bottom of each range bin due to the length of the range bin, approximately 0.05 m. Within the errors bars on these measurements, the plot in figure 5 shows that there is agreement in the mean streamwise flow velocity measured by the CDVP and both ADVs. Using a normal axis regression to compare the data, gave a regression gradient of 0.96 ± 0.06 for the comparison with the ADV-N, with a regression coefficient of 0.999, and a gradient of 1.02 ± 0.11 for the ADV-S with a regression coefficient of 0.998. Testing the significance of the gradient using the t-distribution value gave t=0.667 and t=0.182 for

the ADV-N and ADV-S data respectively, which was less than the 1% t-distribution value of 3.7 for n=8. The regression gradients therefore did not differ significantly from unity at the 99% confidence level.

The triple axis CDVP had the capability to measure the velocity in range bins of approximately 0.05 m over a 1.28 m range. In the present study the CDVP was mounted at 0.8 m above a mean bed location, although the actual height of the range bins above the bed varied over the measurement period due to the migration of bedforms below the instrument package. The range to the bed was determined by identifying when bed echoes contaminated the data. Figure 6 shows the mean streamwise velocity profiles, measured by the triple axis CDVP over the flood period. These profiles show an increase in velocity with increasing height above the bed, with the velocities approaching zero towards the bed as would be expected. Some detailed variations in the shape of the velocity profiles were observed over the flood and this was considered in part due to the migrating bedform beneath the instruments.

(ii)Time series of CDVP data

Figure 7 shows an example from the middle of the flood tide, of a comparison of 100 s of time series of velocity data for a) with flow (u), b) crossflow v, and c) vertical flow w, from adjacent CDVP bins. These plots show what differneces occurred over a 0.06 m vertical range. The velocities are very comparable, and the difference is plotted above the 2 bin time series. To quantify the difference $<|\zeta_d|>/ \tilde{u}$, was calculated, where $<|\zeta_d|>=<|\zeta_i-\zeta_j|>$, ζ represents u, v, or w, i and j represents adjacent range bins, $\tilde{u}=<(|u_i|+|uj|)>/2$, and $<>$ represents an average over a record. The average for $<|\zeta_d|>/ \tilde{u}$ over the flood period gave values of 0.09±0.02 and 0.10±0.02 for u and v respectively. This was considered acceptable for a 0.06 m vertical separation in the measurement volumes and it was probable that spatial de-correlation of the higher frequency velocity components occurred over this separation.

(iii)Comparison of ADV velocities

Before making a comparison of the CDVP with the two ADV instruments, it was considered useful to assess the coherence of the velocities measured by the two ADVs. The ADV-N and the ADV-S were separated vertically by 0.1 m and horizontally in the X direction by 0.12 m. Although a number of analyses were conducted, the main outcome can be illustrated by the results in figure 8a-8c. These scatter plots show

measurements for u, v and w. Regression analysis gave gradients and coefficients of 1.20 ± 0.01 and 0.97 for u, and 1.09 ± 0.03 and 0.93 for v. The gradients are greater than unity due to the ADV-N, the ADV furthest from the bed, being the dependent variable. For w the comparable results were a gradient of 0.8149 and a regression coefficient 0.133, the latter being significantly below that for u and v. This relatively weak correlation in w was considered to be due to the reduced coherency owing to horizontal and vertical separation of the ADV's. Calculation of $<|\zeta_d|>/ \tilde{u}$ gave mean values over the flood for u and v of 0.17±0.01 and 0.16±0.01 respectively. These values are somewhat larger than calculated for the CDVP adjacent range bin analysis and this is ascribed to the vertical and horizontal separation of the ADV's.

(iv) Comparison of the CDVP and ADV time series

Figures 9-14 show an example of a comparison of 100 s of time series of velocity data with flow (u) velocity data from the ADV-N and the CDVP, and the ADV_S and the CDVP respectively, for records 1-8. As can be seen the velocities are very comparable for the records 2-7. Each plot also shows the velocity difference between the instruments with the scale (in ms^{-1}) shown on the ordinate on the right side of the plot. The quantitative difference $<|\zeta_d|>/ \tilde{u}$, was calculated as before and Table 2 shows the results of the differences between the measured u, v and w velocities obtained from the CDVP and the two ADVs at the appropriate heights. The average value of $<|\zeta_d|>/ \tilde{u}$ over the middle of the flood period from 10:29-13:00 UTC was 0.26±0.02, 0.27±0.03 and 0.22±0.02 for u, v and w respectively for the ADV-N comparison and 0.30±0.02, 0.33±0.02 and 0.25±0.02 for u, v and w respectively for the ADV-S comparison. These values for $<|\zeta_d|>/\tilde{u}$ are larger than the differences between measurements in adjacent bins of the CDVP, however the ADV intercomparison was also greater than that between range bins; it is therefore considered that the spatial separation of the ADV's measurement volumes from the CDVP range bins (0.5 m) may account for the increase in $<|\zeta_d|>/\tilde{u}$. The data at the start and end of the flood tide suggests that there was insufficient sediment in suspension at these times to obtain accurate velocity estimates from the CDVP, which shows a limiting factor for the use of the instrument.

Table 2. Quantitative results of the differences between the measured u, v and w velocities obtained from the CDVP and the ADV's

$<\lvert\zeta_d\rvert>/\tilde{u}$ for u Nortek	$<\lvert\zeta_d\rvert>/\tilde{u}$ for v Nortek	$<\lvert\zeta_d\rvert>/\tilde{u}$ for w Nortek
0.4210	0.9357	0.2535
0.2197	0.1964	0.1996
0.2221	0.2019	0.2244
0.2473	0.2058	0.2200
0.2408	0.1975	0.2125
0.2712	0.2331	0.2453
0.3296	0.3130	0.3225
0.8015	0.9726	0.6516
Mean(10:29-13:00)	Mean(10:29-13:00)	Mean(10:29-13:00)
0.2402	0.2070	0.2204

$<\lvert\zeta_d\rvert>/\tilde{u}$ for u Sontek	$<\lvert\zeta_d\rvert>/\tilde{u}$ for v Sontek	$<\lvert\zeta_d\rvert>/\tilde{u}$ for w Sontek
0.5881	0.9870	0.2572
0.2800	0.2527	0.2099
0.2708	0.2641	0.2606
0.2734	0.2650	0.2285
0.2717	0.2501	0.2374
0.3452	0.3025	0.3021
0.5012	0.4965	0.3932
1.2489	1.4914	0.8027
Mean(10:29-13:00)	Mean(10:29-13:00)	Mean(10:29-13:00)
0.2882	0.2669	0.2477

(v) Comparison of the CDVP with the ADV at 16 Hz.

Referring to figure 15; figures 15(a) to 15(c) show scatter plots of the velocity for the CDVP versus the ADVs. The scatter plots in figures 15(a) to 15(c) are comparable with those in figures 8(a) to 8(c), with the u and v data for the CDVP versus the ADV's being clustered about the line of gradient unity and with obvious correlation, and with almost no correlation for the w component of flow. This lack of correlation for the w component is ascribed to the horizontal spatial separation of the CDVP and the ADVs. Both of the ADVs were displaced 0.185 m in the Y direction, crosswise, and 0.405 m and 0.525 m in the X direction, streamwise, respectively for ADV-N and ADV-S from the CDVP measuring volume. Conducting a linear regression on the 16 Hz CDVP and ADV data gave the results shown in Table 3. These were obtained by carrying out a linear regression on each of the 1024 s records over the flood period and forming the mean and standard deviation for the gradient and regression coefficient. For the u component of flow the results show gradients marginally less than unity, although with standard deviations encompass unity, and high regression coefficients. The departure of the gradients from unity could be associated with the bed level and local bedforms.

Although the range bins corresponding to the ADV's measurement volume remained fixed, the height of both the CDVP range bins and ADVs measurement volumes varied with height above the bed within a record and from record to record due to migrating bedforms below the instruments. For the v component the gradients are below unity and with reduced regression coefficients. This may in part be due to the difference in measurement heights as noted above and in some manner associated with spanwise de-correlation of the v component as expressed by the reduced regression coefficients, however, at present this difference is not fully resolved. The w component of flow shows no correlation and this is ascribed to the spatial de-correlation of the 16 Hz velocity time series as discussed above in reference to figure 8c.

Table 3 Table of the mean regression gradients and coefficients for the comparison between the ADV and CDVP velocity measurements. The mean was taken over the 8 records of data throughout the tidal cycle.

	CDVP / ADV-S	CDVP / ADV-N
Regression gradient u	0.95 ± 0.09	0.90 ± 0.09
Regression coefficient u	0.90± 0.06	0.95± 0.03
Regression gradient v	0.80 ± 0.3	0.72 ± 0.2
Regression coefficient v	0.63± 0.2	0.69± 0.2
Regression gradient w	12 ± 23	10 ± 26
Regression coefficient w	-0.002± 0.08	-0.1± 0.12

Figures 16-21 show the CDVP and ADV power spectral density plots for the three components of velocity; figures 16-18 and 19-21 show the comparison with the ADV_N and ADV_S respectively. Figures 22-24 show the probability density functions of the velocities measured by the CDVP and the ADV-S, and figure 25 shows an example of the pdf's of the velocities for the ADV-N from record 4. The u and the v spectra presented in figures 16 and 17, and the pdfs in figures 22 and 23 show CDVP results that compare well with the ADV measurements. There are differences in the spectrum; the CDVP spectra begin to depart from the ADV above about 2 Hz, with the CDVP measuring larger spectral components at the higher frequencies. This common trend suggests that there is a limitation of the present CDVP system, to measure up to the 2

Hz noise floor. The comparison of the w component of flow is less convincing as can be seen in figures 18 and 21. From the discussions above, detailed time series comparisons were expected to be problematic given the negligible regression coefficient. However, it was anticipated that the form of the spectra would give comparable results. As can be seen in figure 18 the spectra are comparable in form, though the CDVP is showing substantially larger spectral components at the lower frequencies, also the probability distribution shown in figure 25 has CDVP velocities spread over a greater range of velocities than the ADV's. These differences may possibly be ascribed to bedform effects, Williams et al 2003a, or may be due to residue components of u and v, after the rotation transformation, still partially contaminating w.

(vi) Comparison of the CDVP with the ADV at 4 Hz post filtering.

The discussion above led to applying a filter to the 16 Hz data to see if this improved the agreement between the two instruments. A Matlab filter design, cheby2, was used. The passband, Wp, and stopband, Ws, edge frequencies of 2 and 4 Hz, respectively, normalized to lie between 0 and 1, were used in a Chebyshev Type II filter order selection, cheb2ord. Cheb2ord(Wp, Ws, Rp, Rs) returns the order N of the lowest order digital Chebyshev Type II filter that loses no more than Rp dB in the passband and has at least Rs dB of attenuation in the stopband. Cheb2ord also returns Wn, the Chebyshev natural frequency to use with Cheby2 to achieve the specifications. Cheby2(N,R,Wn) designs an Nth order lowpass digital Chebyshev filter with the stopband ripple R decibels down and stopband edge frequency Wn. Cheby2 returns the filter coefficients in length N+1 vectors B (numerator) and A (denominator). R was set at 20. The Matlab zero-phase forward and reverse digital filtering, filtfilt was applied to the 16 Hz data, V_16 to generate the filtered data, V_4, ie V_4 = filtfilt(B, A, V_16) filters the data in vector V_16 with the filter described by vectors A and B to create the filtered data V_4. The result has zero phase distortion and magnitude modified by the square of the filter's magnitude response.

Figures 26 and 27 show examples of time series of u, v and w for the CDVP and ADV-N and ADV-S respectively, at 11:29 UCT, where the filtered data is shown beneath the original 16 Hz data. The reduction in noise on the time series plot shows the differences in measurements between the 2 instruments more clearly. Figure 28 shows examples of the PSD generated after the data was filtered for u, v and w from 11:29 for both Sontek (a,b,c) compared with the CDVP, and Nortek(d,e,f), compared with the CDVP. The best

agreement occurs for the u component with the discrepancy between the instruments remaining below 2 Hz for the vertical component.

(vii) Visualisation of the wave and turbulent flow.

Figure 29 illustrates the capability of the CDVP for visualising the flow and is a plot of the velocity vectors including wave and turbulent components. The figure shows the **uw**, **vw** and **uv** velocity vectors, where the individual velocity components were zero meaned, plotted over a 5 second time period, between 0.05 m to 0.7 m above the bed. The length of the velocity vectors is indicated in the figure. A single point measurement instrument such as an ADV can provide the time varying velocity vectors at a single height above the bed, however, the spatial profiling which is achievable with the triple axis CDVP provides a capability to visualise structures in the flow. Such structures can be seen in figure 25 and are probably associated with the wave component of the flow. This type of plot exemplifies the value of developing a three axis CDVP with co-located volumes, since it clearly illustrates the fine scale temporal and spatial flow structures which can be measured in the nearbed flow regime.

(5) Discussion and Conclusions

The three axis CDVP is under development, and this report assesses the capability to date, as demonstrated during the first field deployment. The advantage of the present system over commercially available coherent Doppler profiling systems is the measurement volume for u, v and w are coincident. The co-location of the velocity measurement volume is an essential requirement for many hydrodynamic and sediment process studies.

To summarize the assessment of the CDVP that was made against two commercially available ADV instruments;

1) Initial comparisons of the streamwise mean velocities of the tidal current over a flood period produced encouraging results with CDVP and ADV measurements showing no significant difference.
2) Comparison of the 16Hz CPVP measurements with the ADV observations carried out using linear regression, time series comparisons and differences, power spectral densities and probability distribution functions was hindered to some extent due to the spatial separation of the ADVs and the CDVP measurement volumes and the variable height of the measurement volumes above the bed due to bedform migration.
3) Allowing for (2), the results showed very comparable measurements for u, comparable observations for v and poor agreement for w.
4) With an operating frequency of 500 kHz, the results suggest that the minimum concentration of suspended sediment required to obtain accurate velocity estimates is 0.01 g/l. (see Appendix 1)
5) Two observations on the u, v, CDVP comparisons with the ADV were that the regression plots yielded gradients less than unity and the power spectra for the CDVP appeared to be reaching a noise floor above about 4 Hz.
6) The reduced gradients, for u, 0.95±0.1 and 0.90±0.1, was considered to be possibly due to the spatial separation and local bed height variation, however, the lower gradients for v, 0.80±0.3 and 0.72±0.2, were not so readily reconciled.
7) The flattening off of the power spectral density above about 4 Hz seems to be a limitation of the system at the present stage of development, as confirmed by the agreement shown between the instruments after the data was filtered to pass frequencies below 4 Hz.

8) The w component of the CDVP and the ADVs were temporally uncorrelated, this was unsurprising given the spatial separation, and the results from the inter-comparison of the two ADV measurements.
9) The differences in the power spectral densities and probability density functions were more difficult to explain; they seemed to be indicating some contamination of the vertical component of the flow by the horizontal components.

Although the present assessment of the triple axis CDVP was limited by the lack of co-location of the ADV and CDVP measuring volumes, the experimental setup enabled as assessment of the capability of the CDVP in a marine setting. The results were generally positive and supported the concept of using acoustics to obtain non-intrusive, high spatial and temporal resolution profiles of co-located three axis velocity measurements, in a nearshore coastal environment. With the existing results, on-going developments require consideration of the transmit transducer operating frequency being increased to 1 MHz, to reduce the noise level and it is also recommended that a more accurate approach of modelling the centre of the intersecting beam patterns could be investigated in future (see for example Zedel & Hay, 2002), for obtaining the position of each velocity reading.

Acknowledgements

The work was supported by the European MAST III project 'Inlet Dynamics Initiative Algarve' (INDIA), contract MAS3-CT97-0106, and NERC. Marine Electronics Ltd assisted in the transducer development and Peter Hardcastle developed the electronics for the current system. Thanks to Alex Souza for helpful discussions.

References

Betteridge, K.F.E., P.D.Thorne, P.S.Bell, 2002: Assessment of acoustic coherent Doppler and cross-correlation techniques for measuring near-bed velocity and suspended sediment profiles in the marine environment. *J. Atmosph and Oceanic Tech.* **19** (3) 367-380.

Betteridge, K.F.E., P.S.Bell, P.D.Thorne, J.J.Williams, 200*: Evaluation of a triple axis Coherent Doppler Velocity Profiler for measuring near-bed flow: A Field Study. *J. Atmosph and Oceanic Tech.* in press, 2005.

Hardcastle, P.J., 1994: A high resolution near-bed coherent acoustic Doppler current profiler for measurement of turbulent flow, *Proc. 6th Int. Conf. on Electronic Engineering in Oceanography,* (London) Conference Publication 394, 73-76.

Hurther, D and U. Lemmin, 1998: A constant-beam-width transducer for 3D acoustic Doppler profile measurements in open-channel flows, *Meas. Sci. Technol.*, **9**, 1706-1714.

Hurther, D and U. Lemmin, 2001: A Correction Method for Turbulence Measurements with a 3D Acoustic Doppler Velocity Profiler, *J. Atmosph and Oceanic Tech.* **18** (3) 446-458.

Rolland, T and U. Lemmin, 1997: A two-component acoustic velocity profiler for use in turbulent open-channel flow *J. Hydr. Research,* **35**(4), 545-562.

Lhermitte, R., and R. Serafin, 1984: Pulse-to-Pulse Coherent Doppler Sonar Signal Processing Techniques, *J. Atmosph and Oceanic Tech.*, **1**, (4) 293-308.

Thorne P.D. and D. Hanes, 2002: A review of acoustic measurement of small scale sediment processes. *Contin. Shelf Res.* **22**, 603-632.

Thorne P.D. and J. Taylor, 2000: Acoustic measurements of boundary layer flow and sediment flux. *J. Acoust. Soc. Am.*, **108** (4) 1568-1581.

Veron, F. and W.K. Melville, 1999; Pulse-to-Pulse Coherent Doppler Measurements of Waves and Turbulence, *J. Atmosph and Oceanic Tech.*, **16**, 1580-1596.

Voulgaris, G, and J.H. Trowbridge, 1998: Evaluation of the Acoustic Doppler Velocimeter (ADV) for Turbulence Measurements. *J. Atmosph and Oceanic Tech.*, **15**, 272-289.

Williams, J.J., P.S. Bell and P.D. Thorne, 2003a: Field measurements of flow fields and sediment transport above mobile bed forms, J. Geophys . Res., **108, (C4),** 6-36.

Williams, J.J., P.S. Bell, J.D. Humphery, P.J. Hardcastle and P.D.Thorne, 2003b: New approach to measurement of sediment processes in a tidal inlet, *Contin. Shelf Res.* **23**, 1239-1254.

Wilson, R.A. Thorne, P.D., Williams, J.J., Bell, P.S., and Hardcastle, P.J., 2000: An evaluation of a 3D acoustic coherent Doppler current profiler in the marine environment Zakharia, M.E. (Ed) In: Proceedings of the 5 th European Conference on Underwater Acoustics, 10-13 July 2000, Lyon, pp 627-632.

Zedel, L., A.E. Hay, R.Cabrera & A Lohrmann, 1996: Performance of a single beam pulse to pulse coherent Doppler profiler, *IEEE J. Ocean. Eng.* **21**, 290-297.

Zedel, L. and A.E. Hay, 1999: A Coherent Doppler Profiler for High-Resolution Particle Velocimetry in the Ocean: Laboratory Measurements of Turbulence and Particle Flux. *J. Atmosph and Oceanic Tech.* **16** 1102-1117.

Zedel, L. and A.E. Hay, 2002: A Three Component Bistatic Coherent Doppler Velocity Profiler: Error Sensitivity and System Accuracy. *IEEE J. Ocean. Eng.* **27**, 717-725.

Appendix 1 :

Grain sizes measured by pumped sampling on day of Doppler operation

Time	Tide	sample	C (g/l)	z (m), nominal
10:00	FLOOD	r11	0.0327	0.01
		r12	0.0308	0.02
		r13	0.0286	0.04
		r14	0.0299	0.08
		r15	0.0189	0.16
		r16	0.0140	0.32
		r17	0.0108	0.64
11:00	FLOOD	r21	0.0544	0.01
		r22	0.0497	0.02
		r23	0.0479	0.04
		r24	0.0381	0.08
		r25	0.0270	0.16
		r26	0.0188	0.32
		r27	0.0142	0.64
12:00	FLOOD	r31	0.0656	0.01
		r32	0.0579	0.02
		r33	0.0522	0.04
		r34	0.0491	0.08
		r35	0.0340	0.16
		r36	0.0212	0.32
		r37	0.0158	0.64
13:30	FLOOD	r41	0.1760	0.01
		r42	0.1114	0.02
		r43	0.1484	0.04
		r44	0.1234	0.08
		r45	0.0683	0.16
		r46	0.0354	0.32
		r47	0.0084	0.64

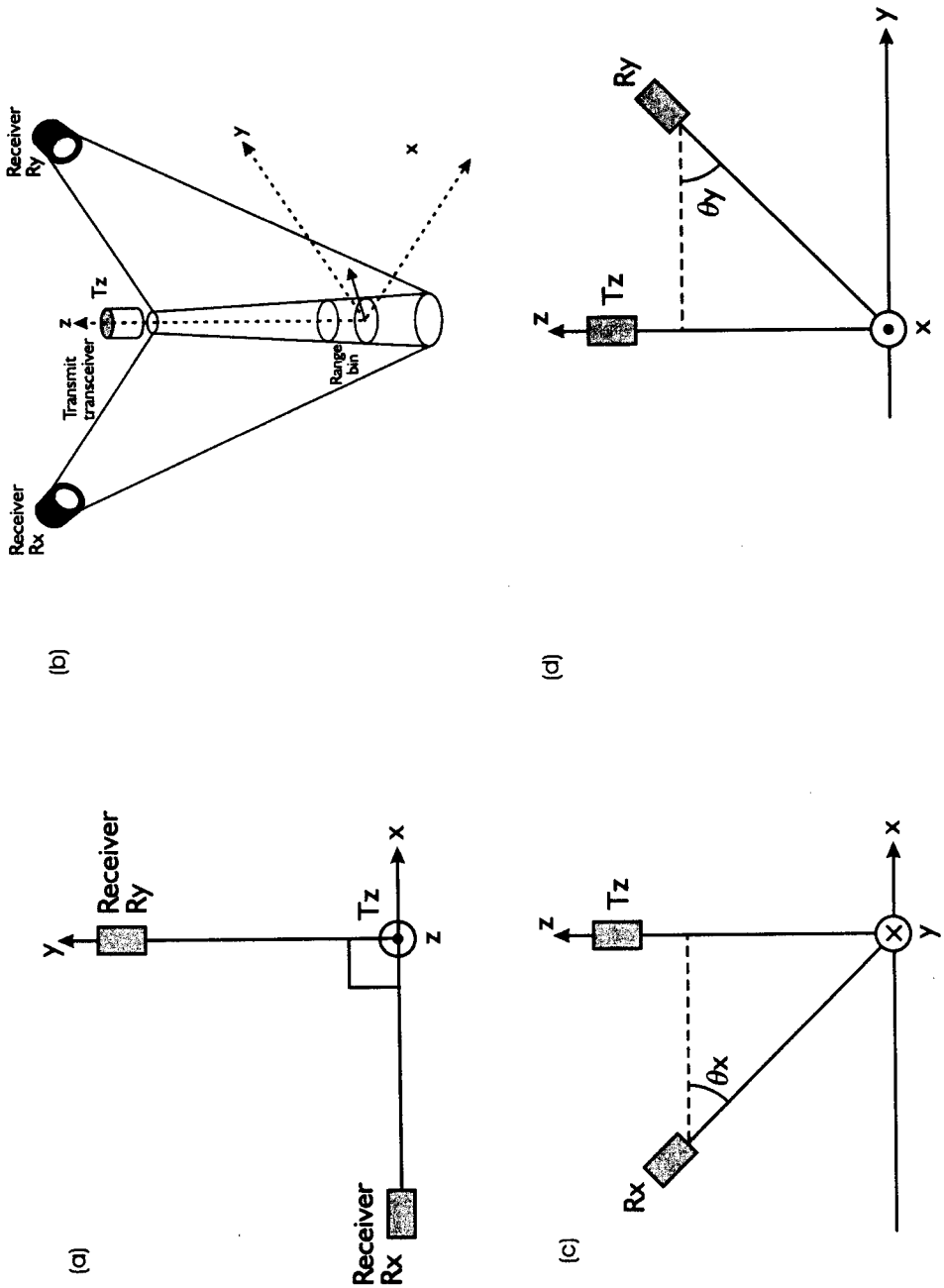

Figure 1. Figures (a) (c) and (d) are projections of the relationships between the transducer locations and the volume insonified at one range bin in the X-Y, X-Z and Y-Z planes respectively. Figure (b) shows the 3D impression of the arrangement

(a)

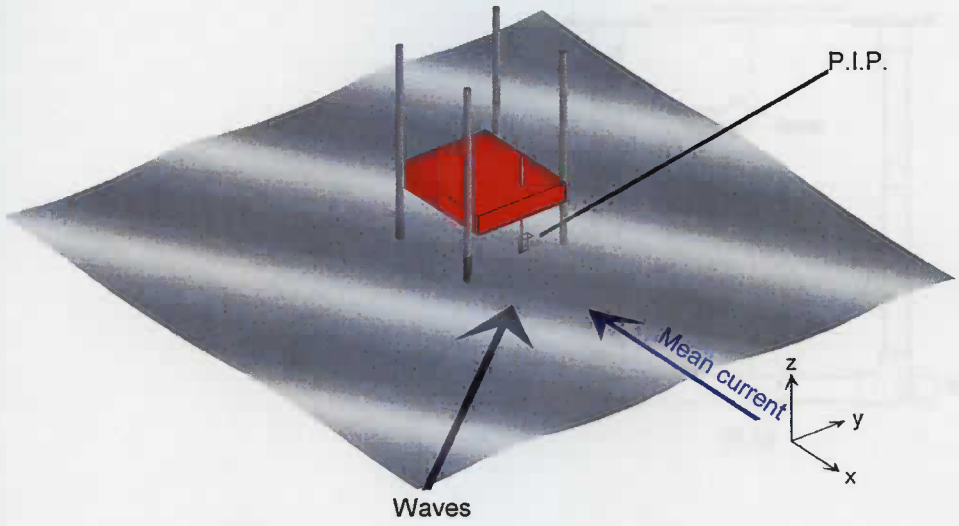

(b)

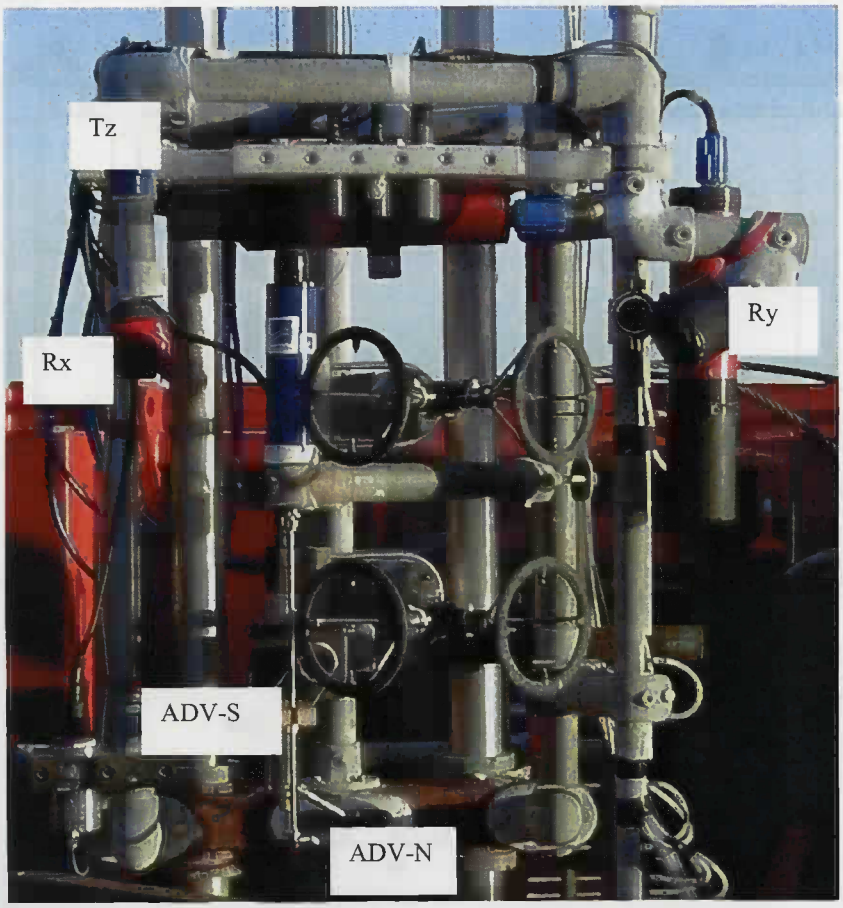

Figure 2 Figure 2a shows the diagram of the PIP relative to the current and wave directions, and the orthogonal axes X, Y and Z. The photograph in figure 2b shows the instrument frame that was deployed for the field work. The components of the triple axis CDVP and the two ADVs are indicated in the picture.

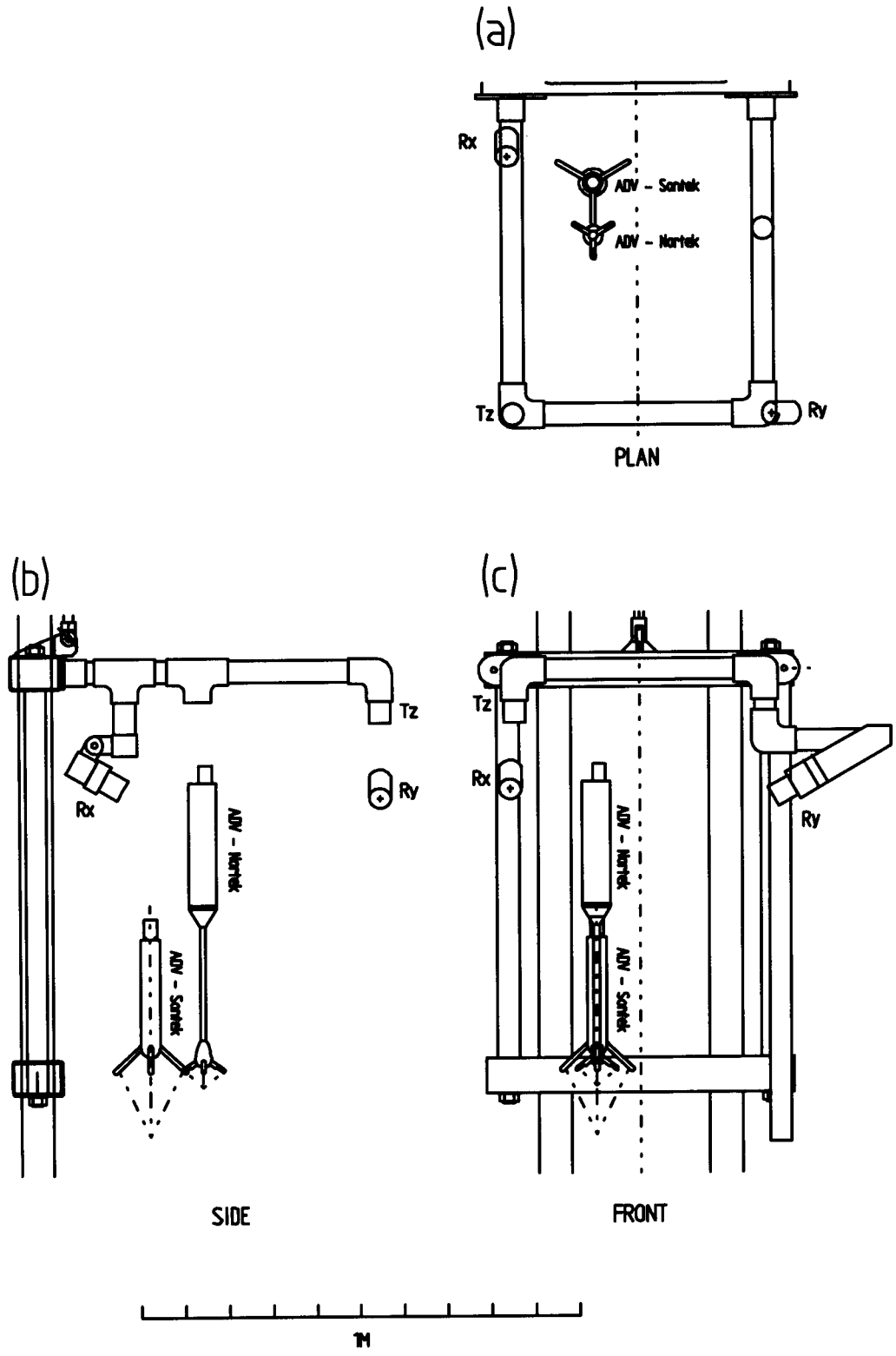

Figure 3 This diagram shows the location of the instruments on the frame (a) plan view in the (X,Y) plane, (b) side view in the (X,Y) plane and (c) front view in the (Y,Z) plane. The relative positions are given in table 1.

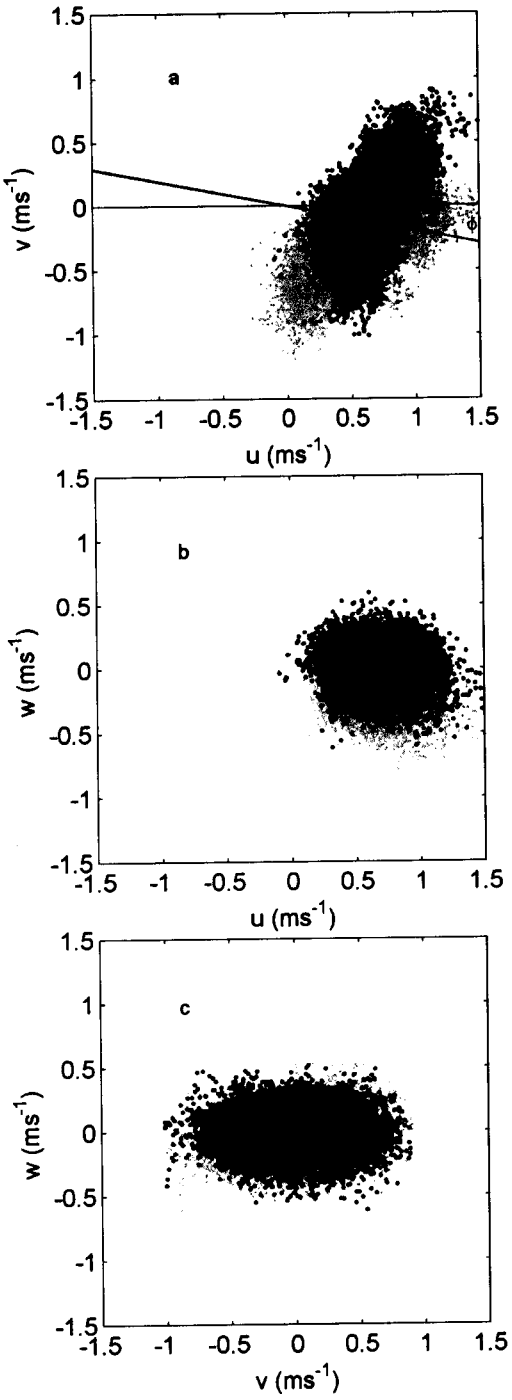

Figure 4 This figure shows how the data was rotated to correct for misalignment relative to the main flow in the vertical and horizontal planes. Figure 4a shows the measured, u_m and v_m, and rotated, u and v, velocity data plotted in grey and black respectively. Similarly v and w, and u and w are shown in figures 4b and 4c. The rotation angle, φ, is marked in 4(a).

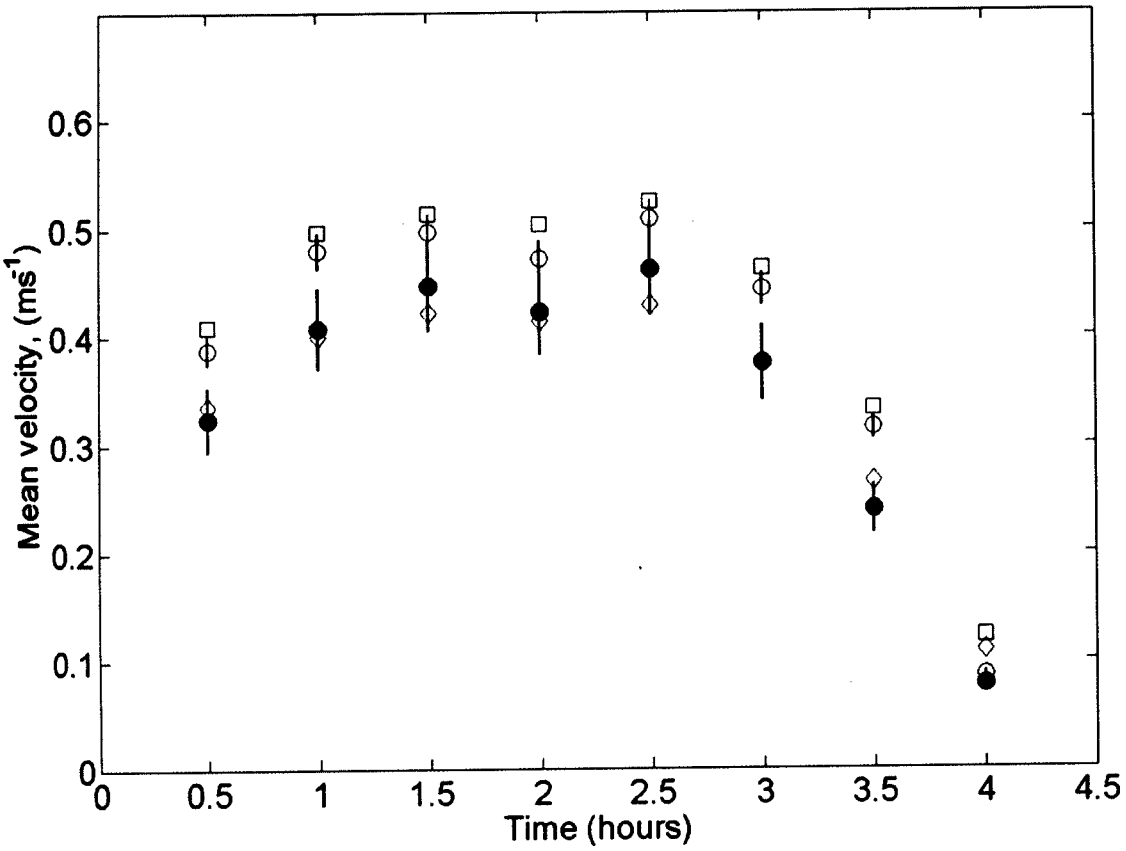

Figure 5 The plot shows the mean current measured by the CDVP and also the two ADVs over a 3.5 hour time period. The CDVP velocity measurements shown are at a nominal height above the bed of 0.07 m (•) and 0.18 m (○). These range bins were the closest to the measurement volumes of the ADVs, at nominally 0.08 m (◊) and 0.18 m (□) respectively above the bed.

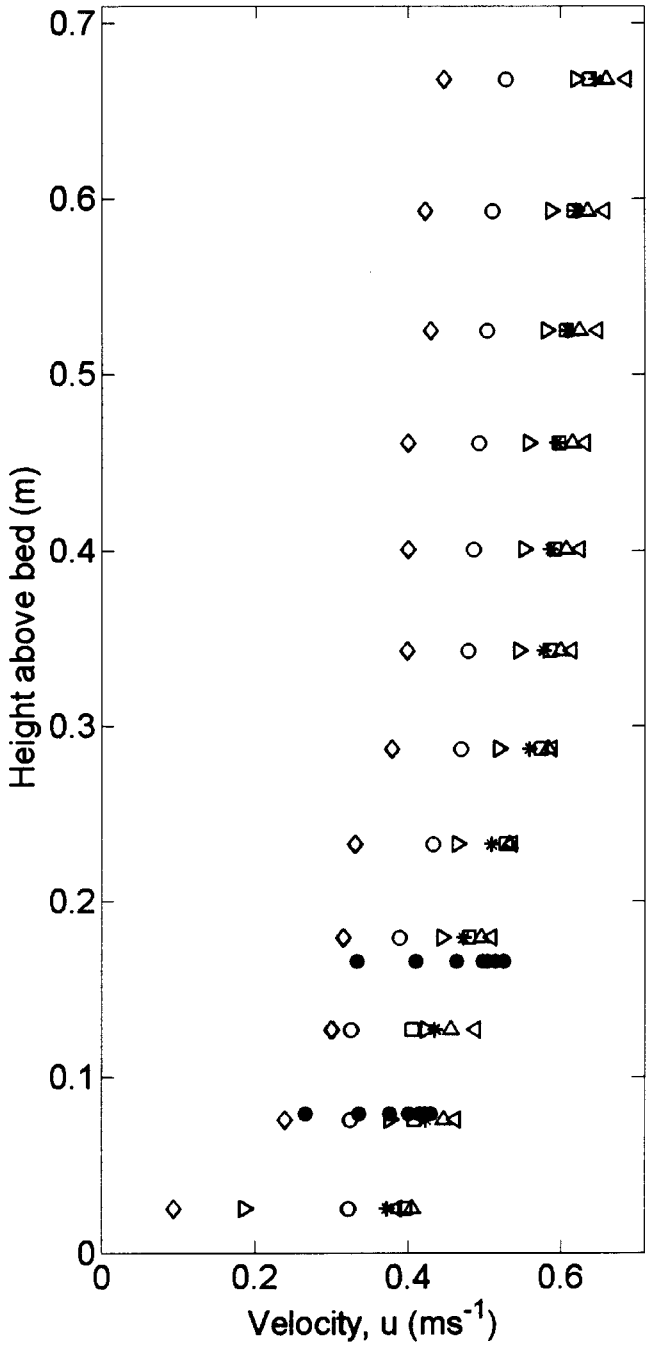

Figure 6 Velocity profile measured by the CDVP over a flood cycle from 09:59-13:59 UTC (o 09:59 □10:29 ▲10:59 *11:29 ◄11:59 ►12:29 and ◊13:59) The different symbols enable the shape of the velocity profiles to be distinguished over the tidal cycle. The measurements obtained with the ADVs are also shown (•).

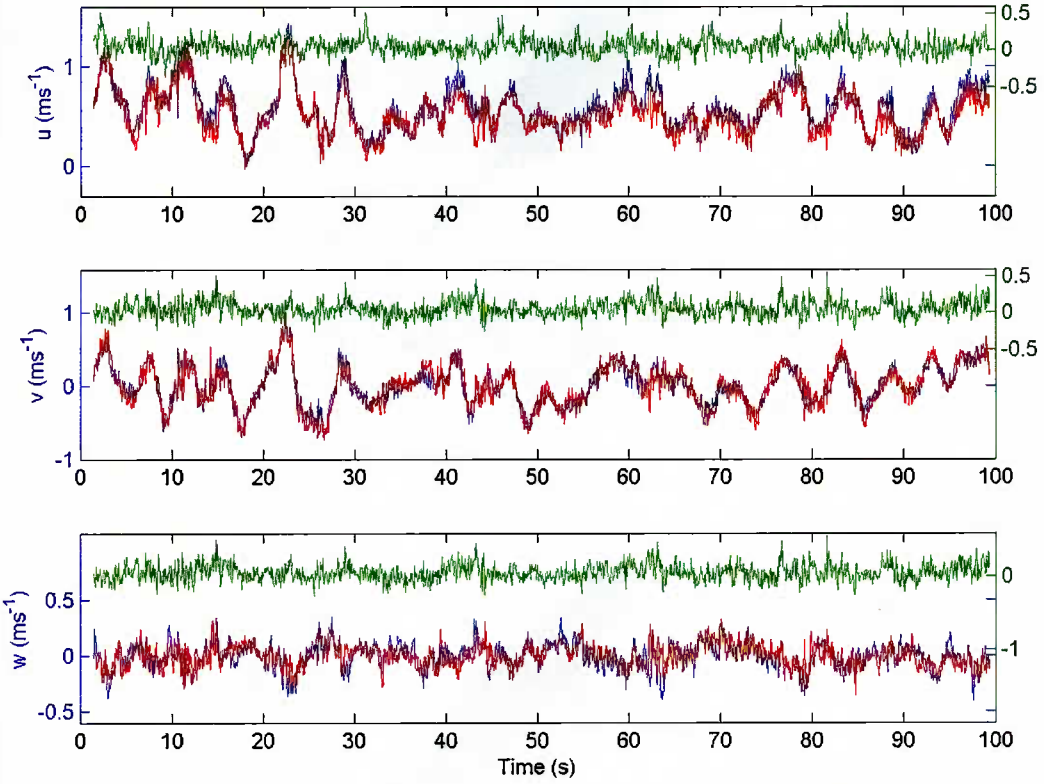

Figure 7 Time series of velocities measured by the CDVP at 2 heights above the bed for record 4, at 11:29, showing u, v and w. The differences are shown in green on a different axis whose scale is shown on the right side of the plot.

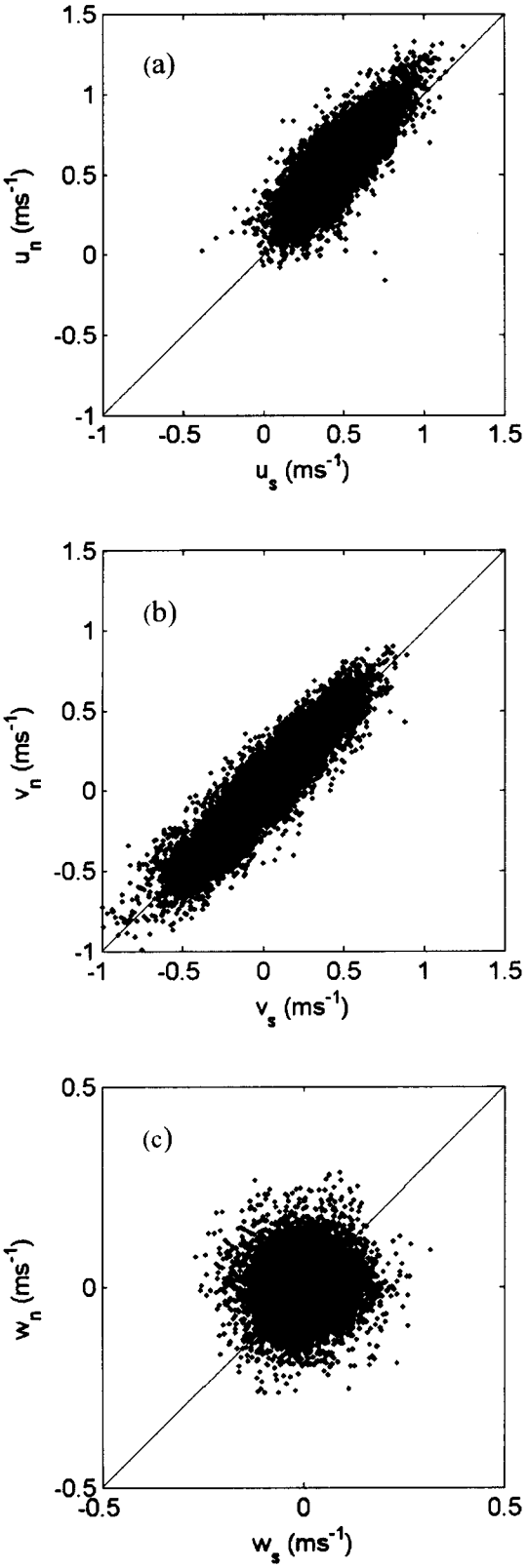

Figure 8 These are plots of the regression of velocities measured by the ADV-S versus those from the ADV-N where (a) is for u, (b) shows v and (c) shows w. The suffix n identifies the Nortek ADV as the ordinate.

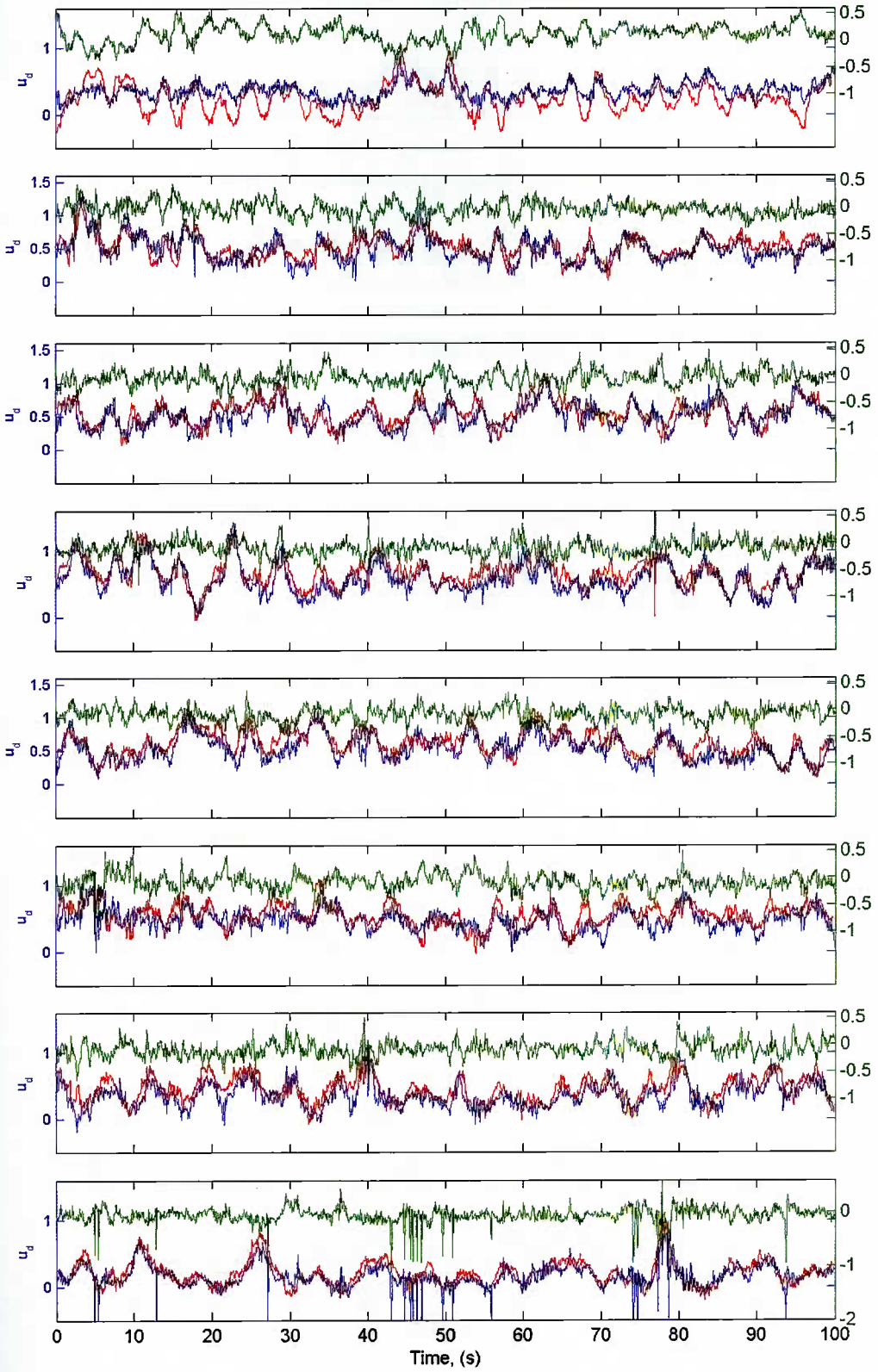

Figure 9 The plots show 100s time series of the with-flow velocity, u, for the CDVP (blue) at the height closest to the ADV-N (red), and the difference plotted in green with the scale shown on the right side of the plot.

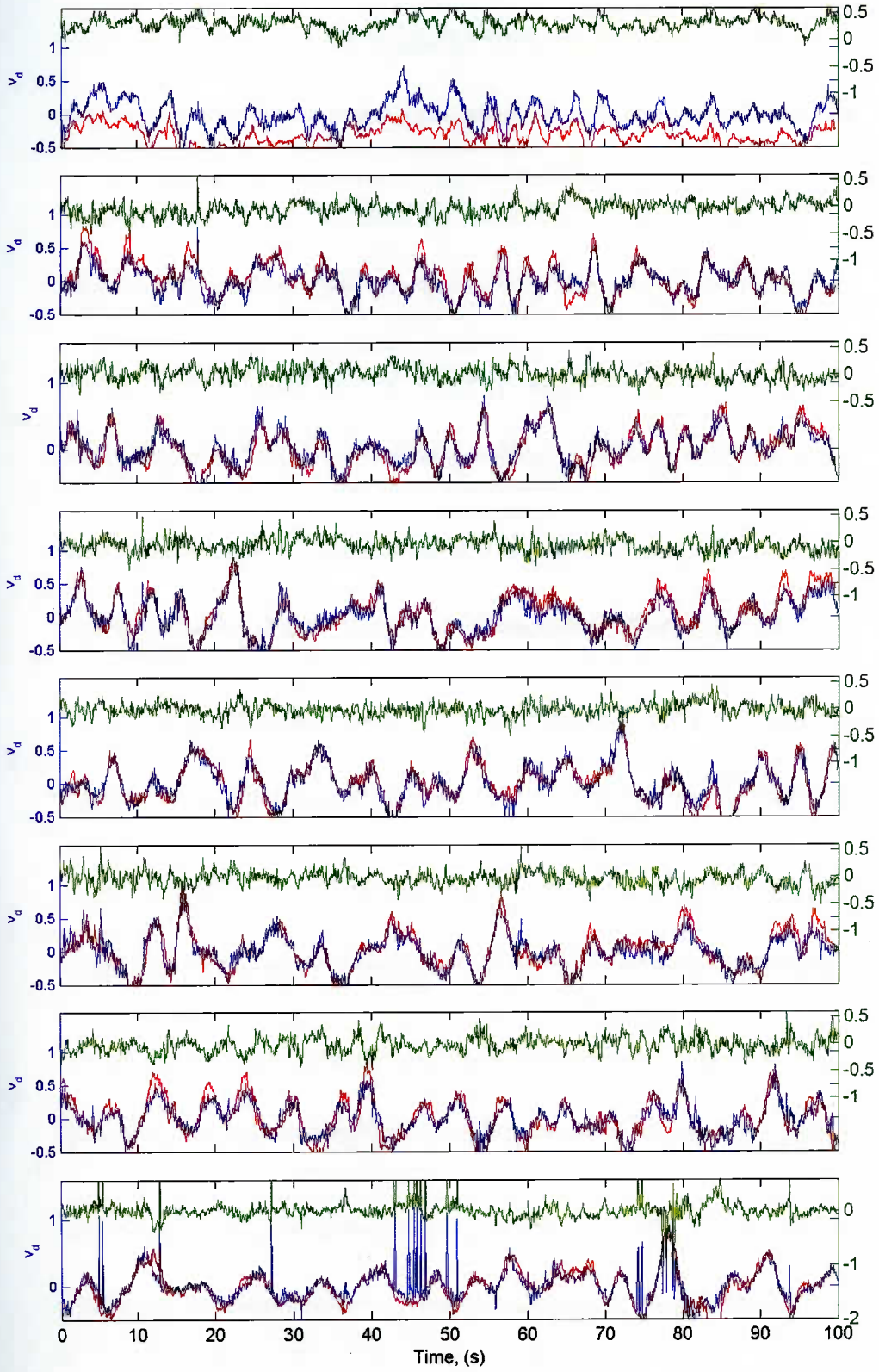

Figure 10 The plots show 100s time series of the cross-flow velocity, v, for the CDVP (blue) at the height closest to the ADV-N (red), and the difference plotted in green with the scale shown on the right side of the plot.

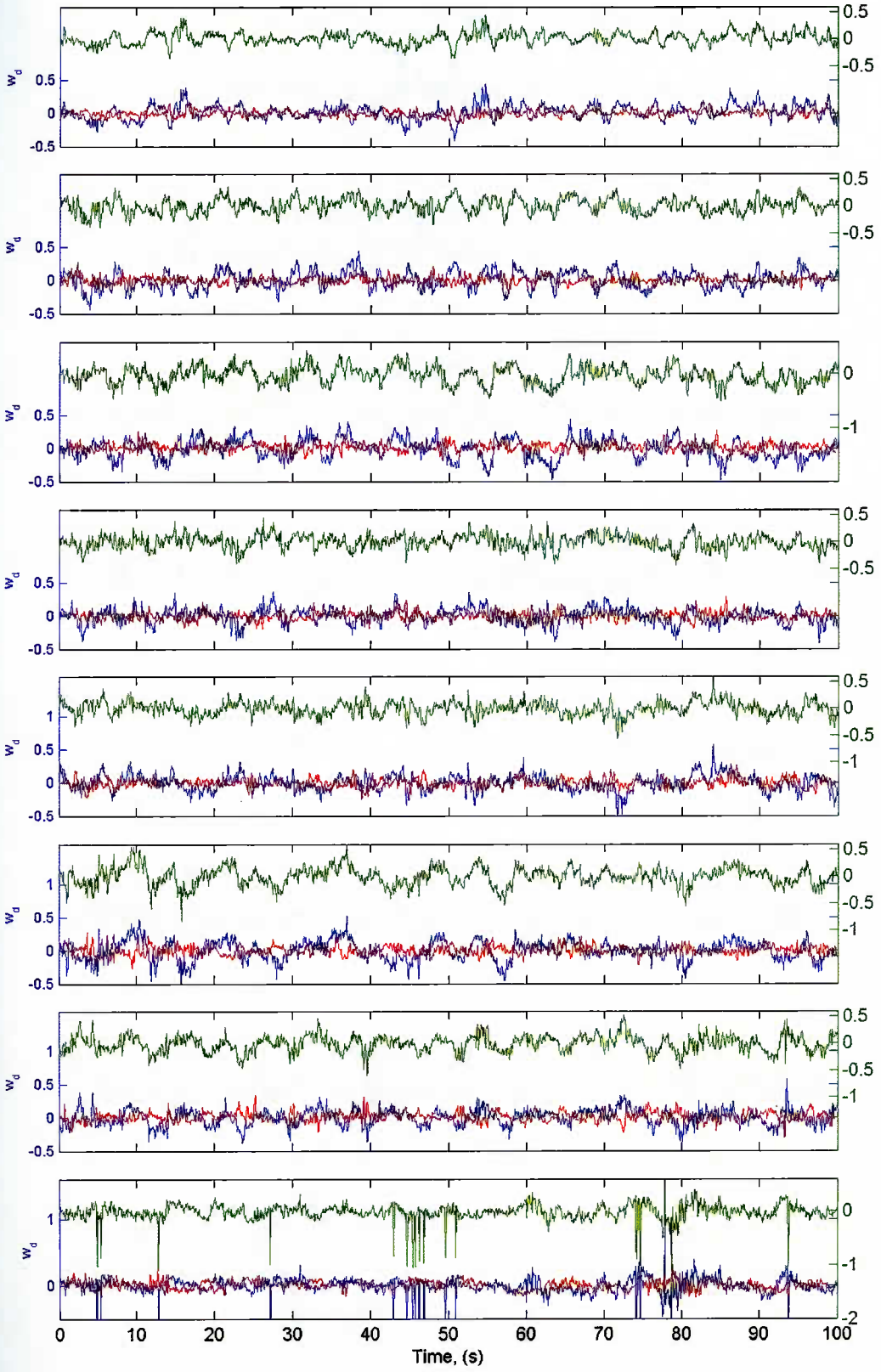

Figure 11 The plots show 100s time series of the vertical velocity, w, for the CDVP (blue) at the height closest to the ADV-N (red), and the difference plotted in green with the scale shown on the right side of the plot.

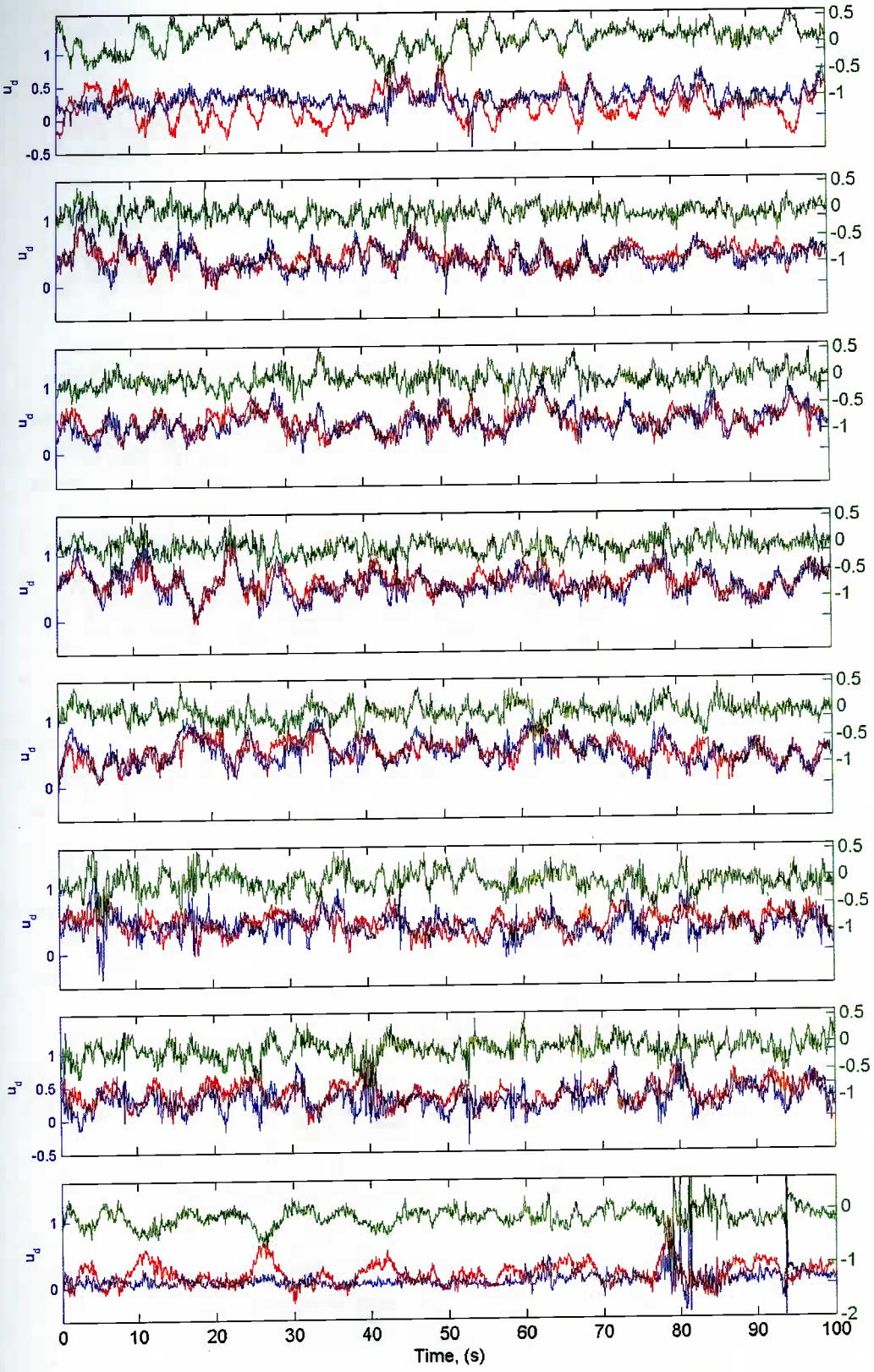

Figure 12 The plots show 100s time series of the with-flow velocity, u, for the CDVP (blue) at the height closest to the ADV-S (red), and the difference plotted in green with the scale shown on the right side of the plot.

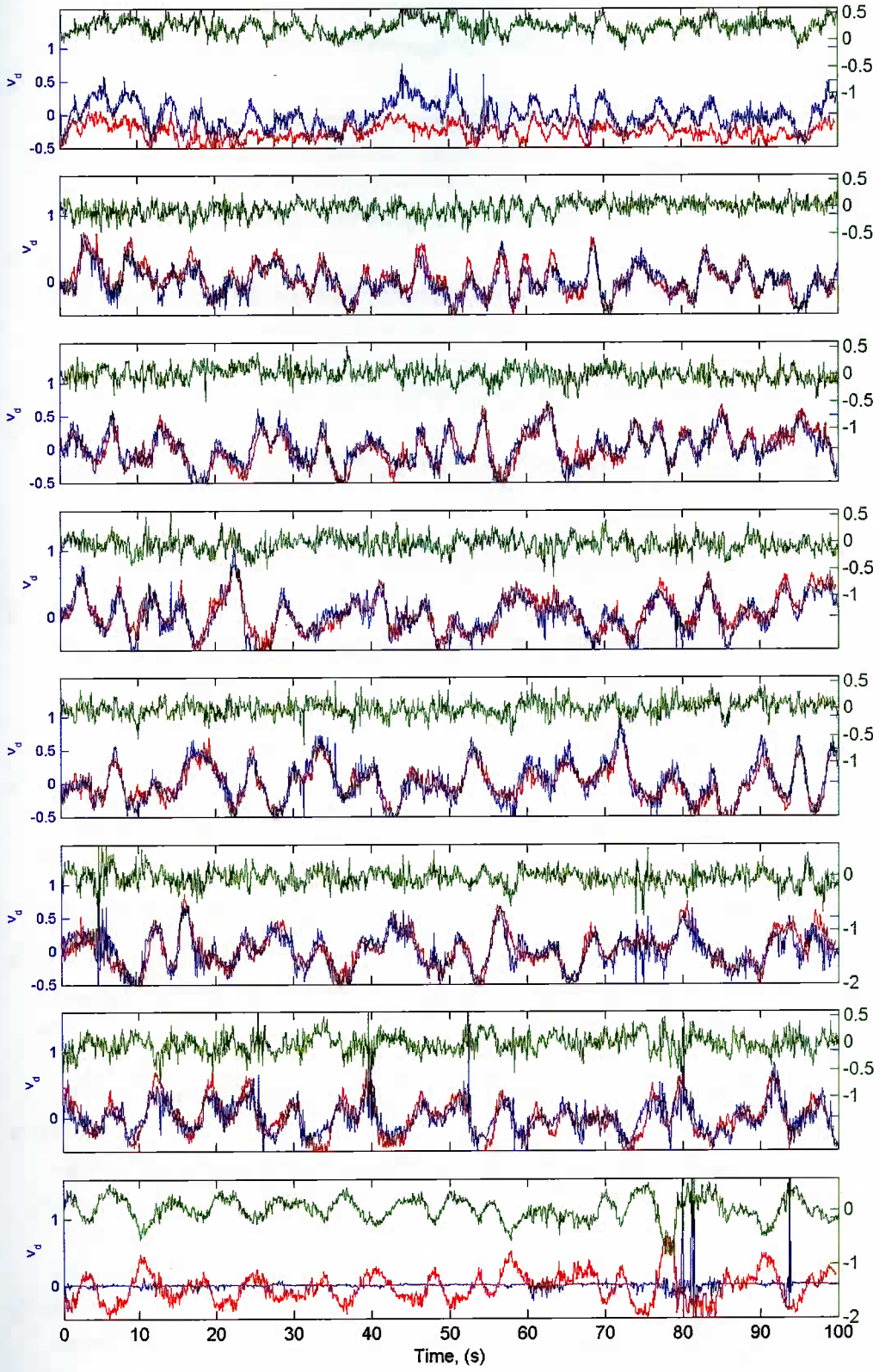

Figure 13 The plots show 100s time series of the cross-flow velocity, v, for the CDVP (blue) at the height closest to the ADV-S (red), and the difference plotted in green with the scale shown on the right side of the plot.

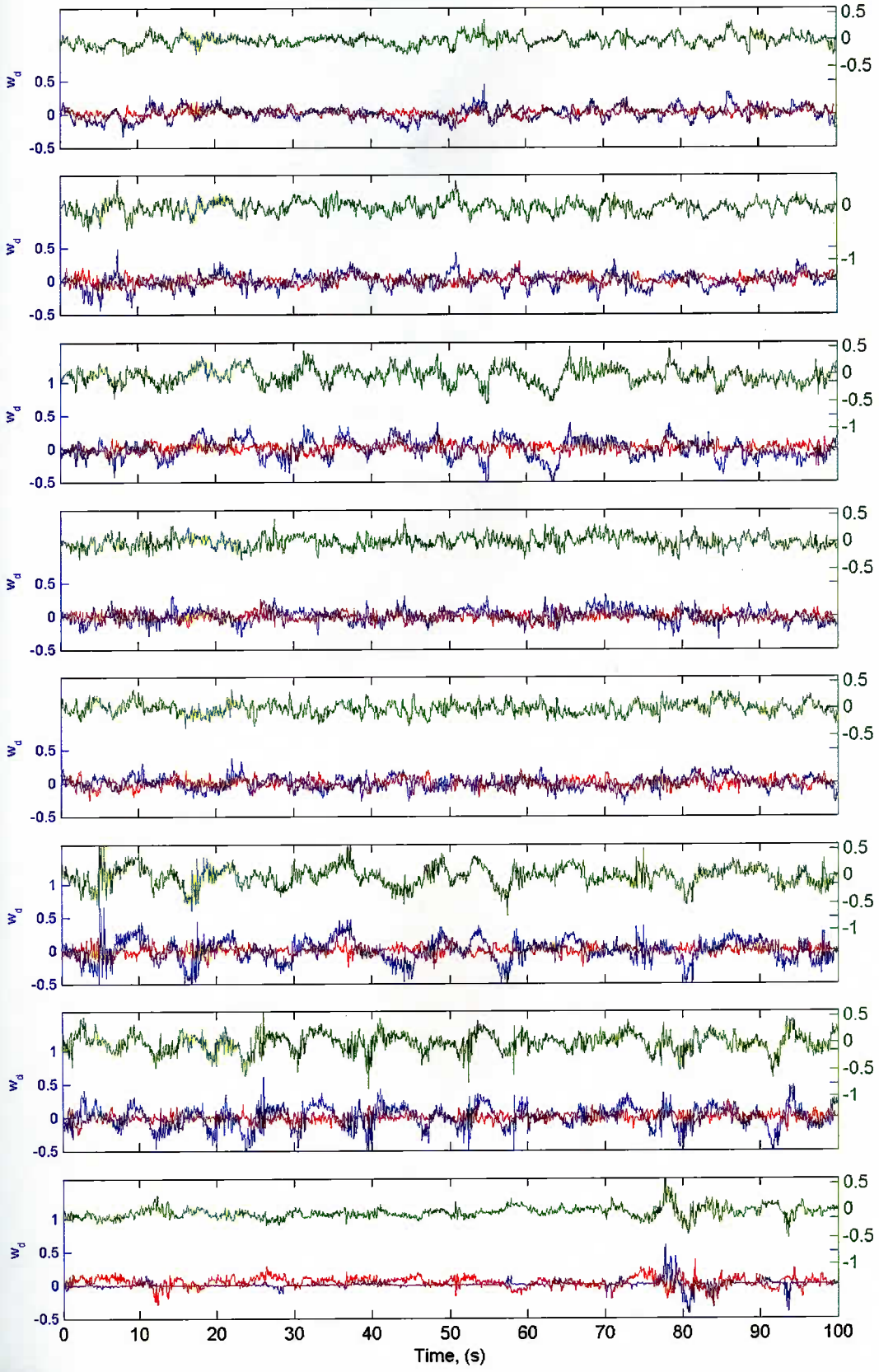

Figure 14 The plots show 100s time series of the vertical velocity, w, for the CDVP (blue) at the height closest to the ADV-S (red), and the difference plotted in green with the scale shown on the right side of the plot.

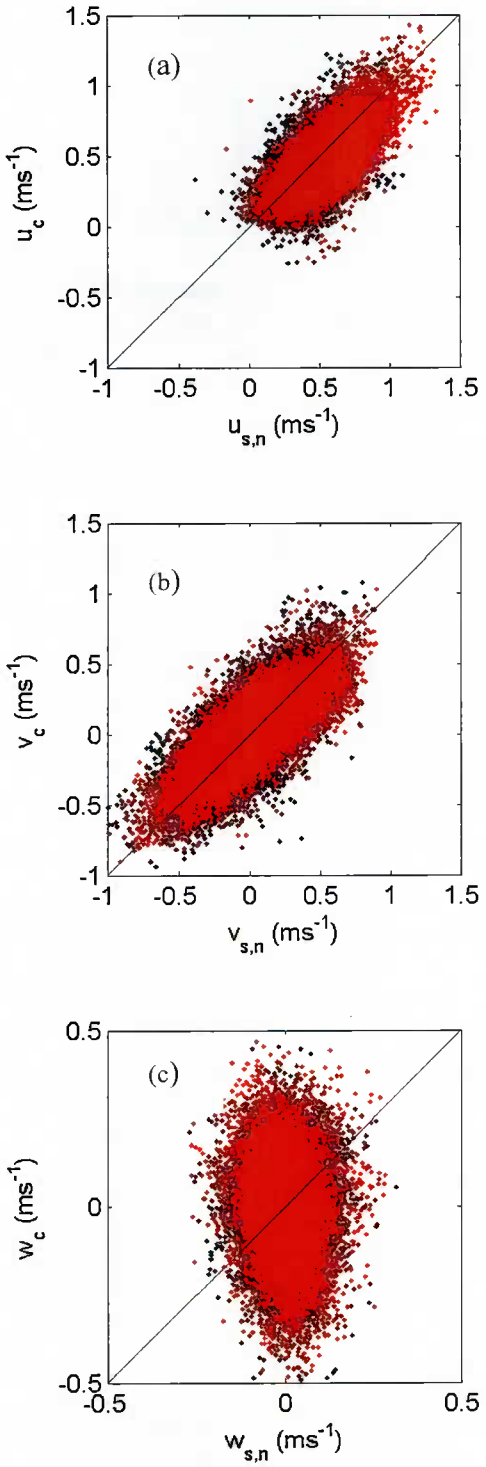

Figure 15 The figure shows regression scatter plots of velocity measured by ADV-S versus CDVP velocities (in black), and scatter plots of ADV-N velocities versus CDVP velocities (in red), where (a) is u, (b) is v and (c) is w.

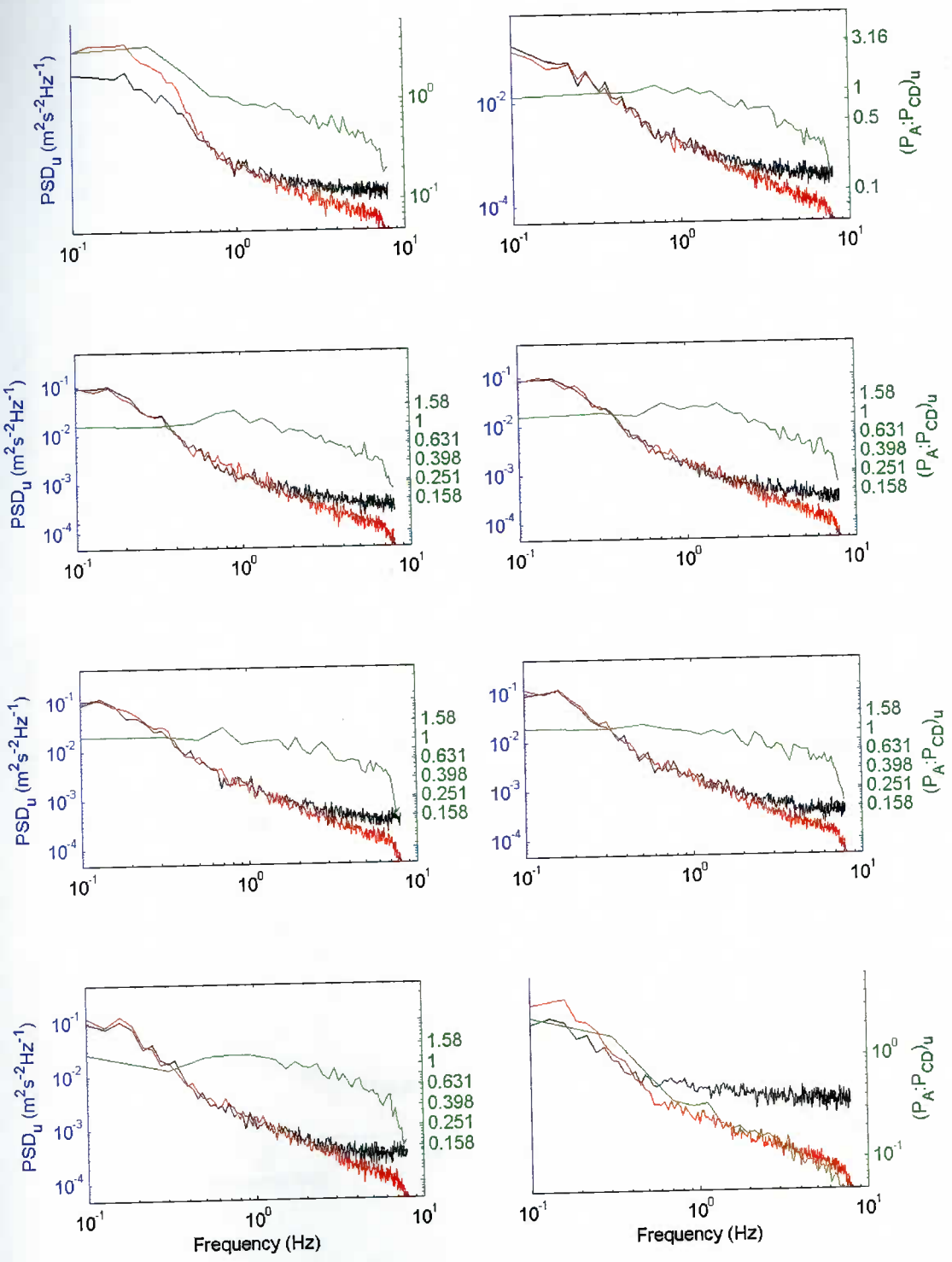

Figure 16. The power spectra of the zero-mean u velocities are plotted in red for the ADV_N and black for the CDVP; the ratio of the spectra is shown by the green plot, with the axis scale indicated on the right side of the figure.

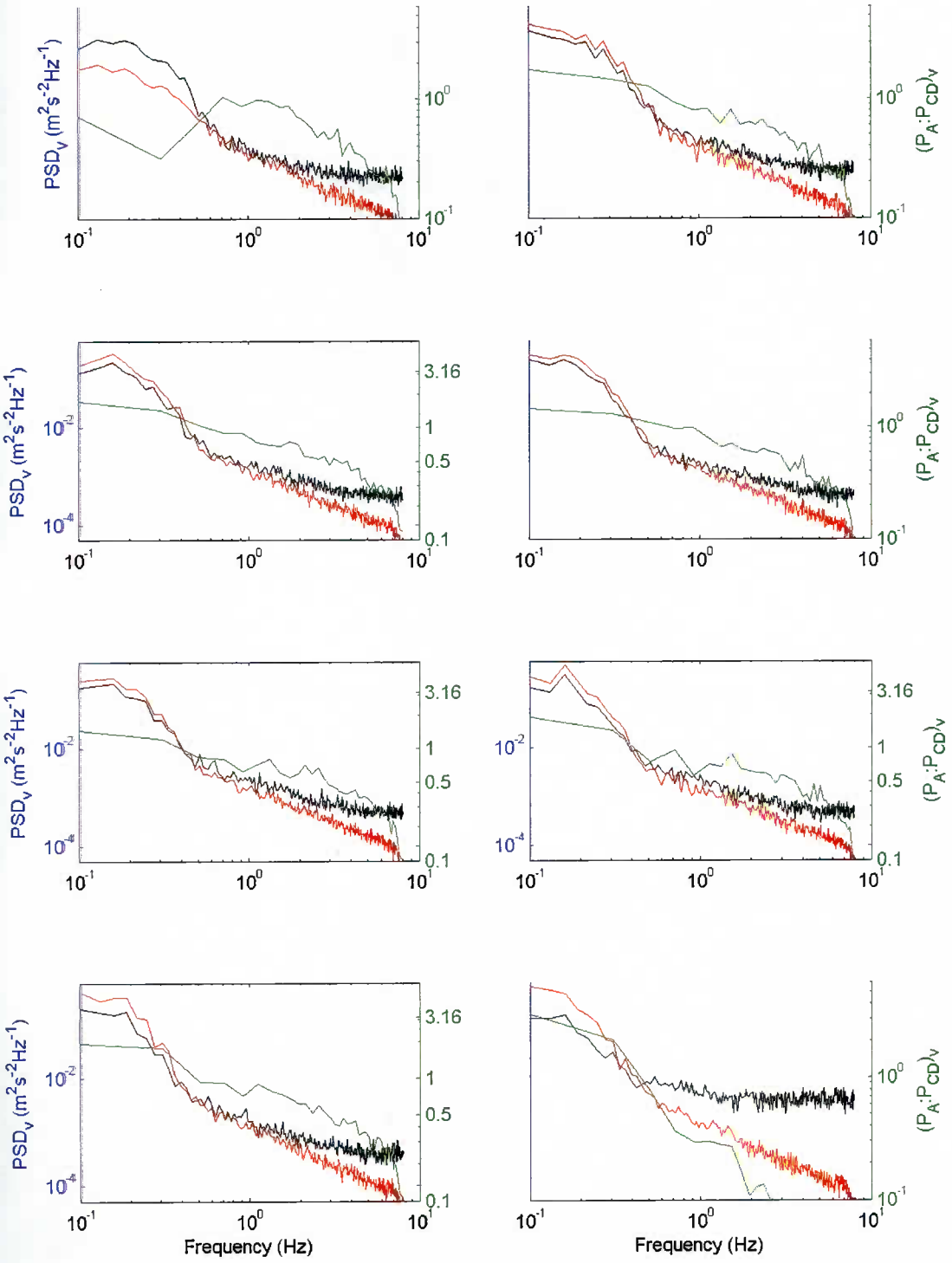

Figure 17. The power spectra of the zero-mean v velocities are plotted in red for the ADV_N and black for the CDVP; the ratio of the spectra is shown by the green plot, with the axis scale indicated on the right side of the figure.

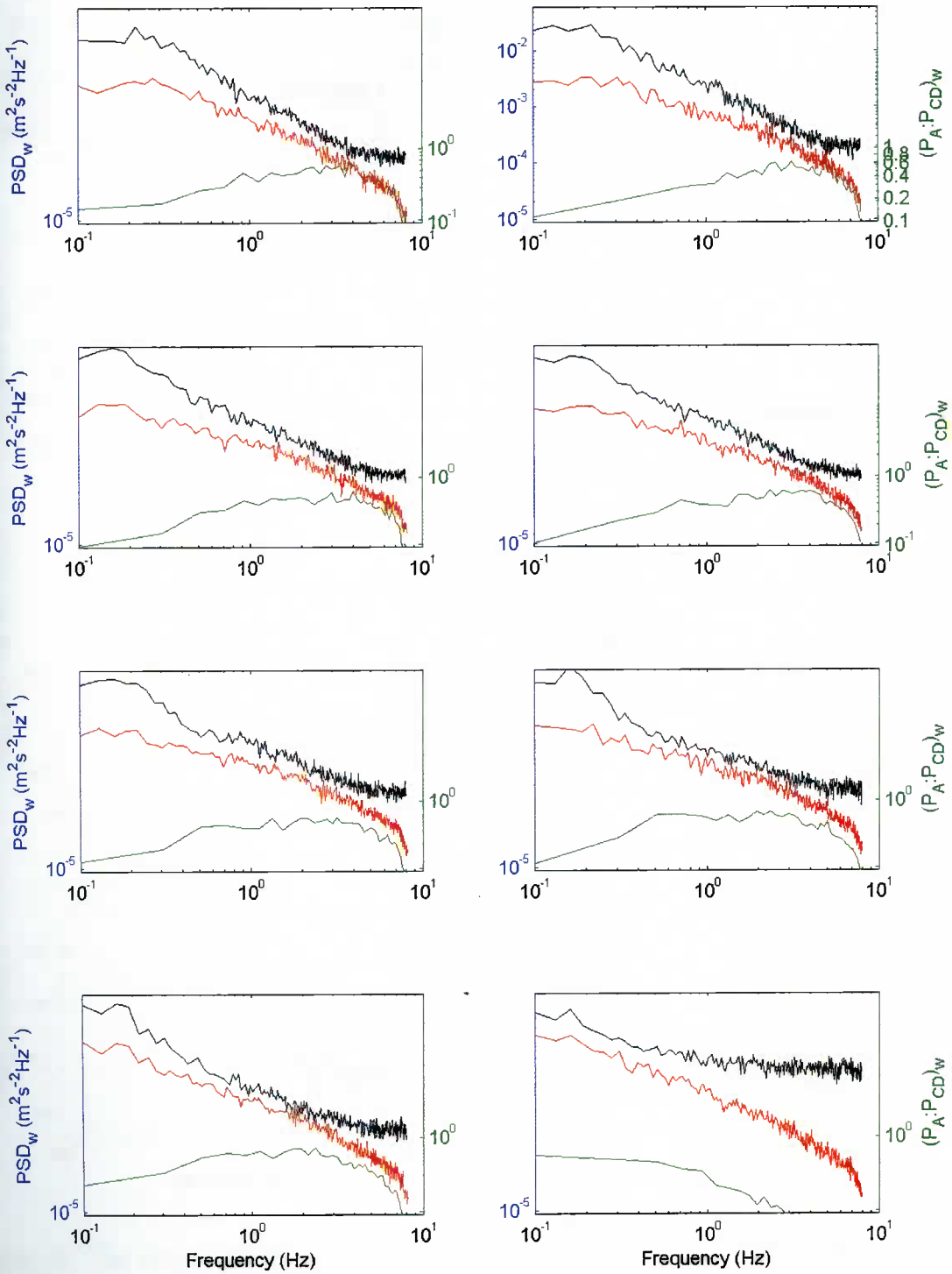

Figure 18. The power spectra of the zero-mean w velocities are plotted in red for the ADV_N and blue for the CDVP; the ratio of the spectra is shown by the green plot, with the axis scale indicated on the right side of the figure.

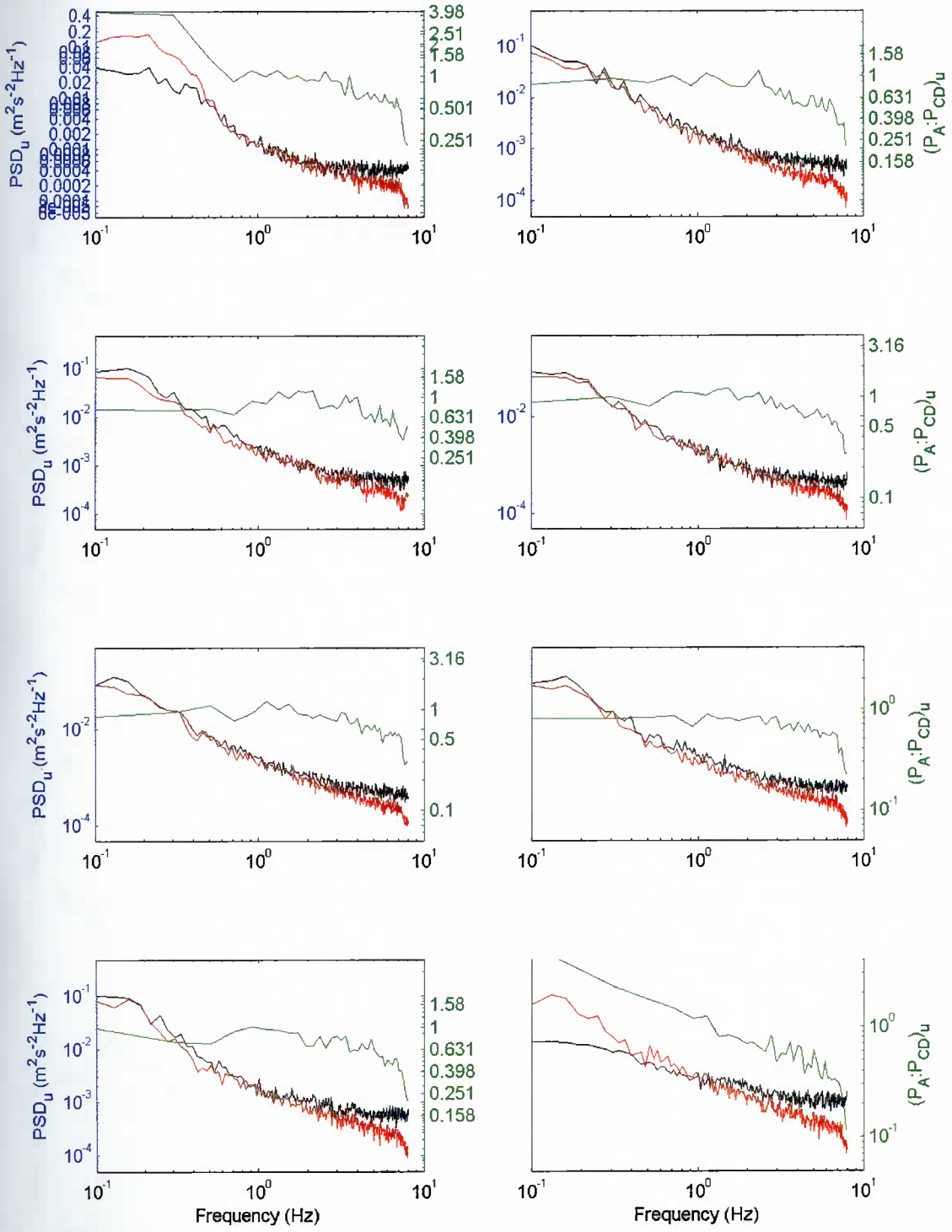

Figure 19. The power spectra of the zero-mean u velocities are plotted in red for the ADV_S and black for the CDVP; the ratio of the spectra is shown by the green plot, with the axis scale indicated on the right side of the figure.

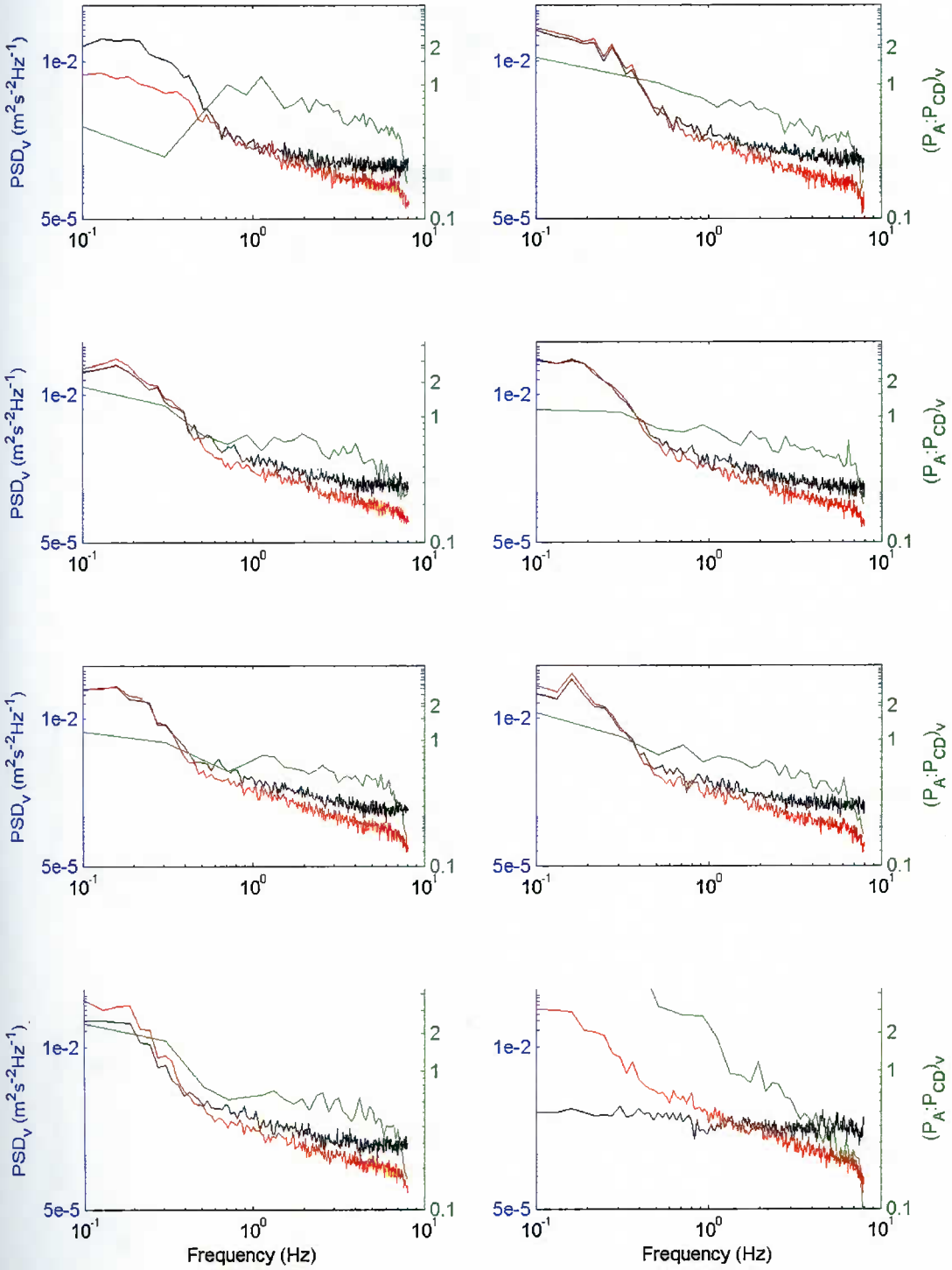

Figure 20. The power spectra of the zero-mean v velocities are plotted in red for the ADV_S and black for the CDVP; the ratio of the spectra is shown by the green plot, with the axis scale indicated on the right side of the figure.

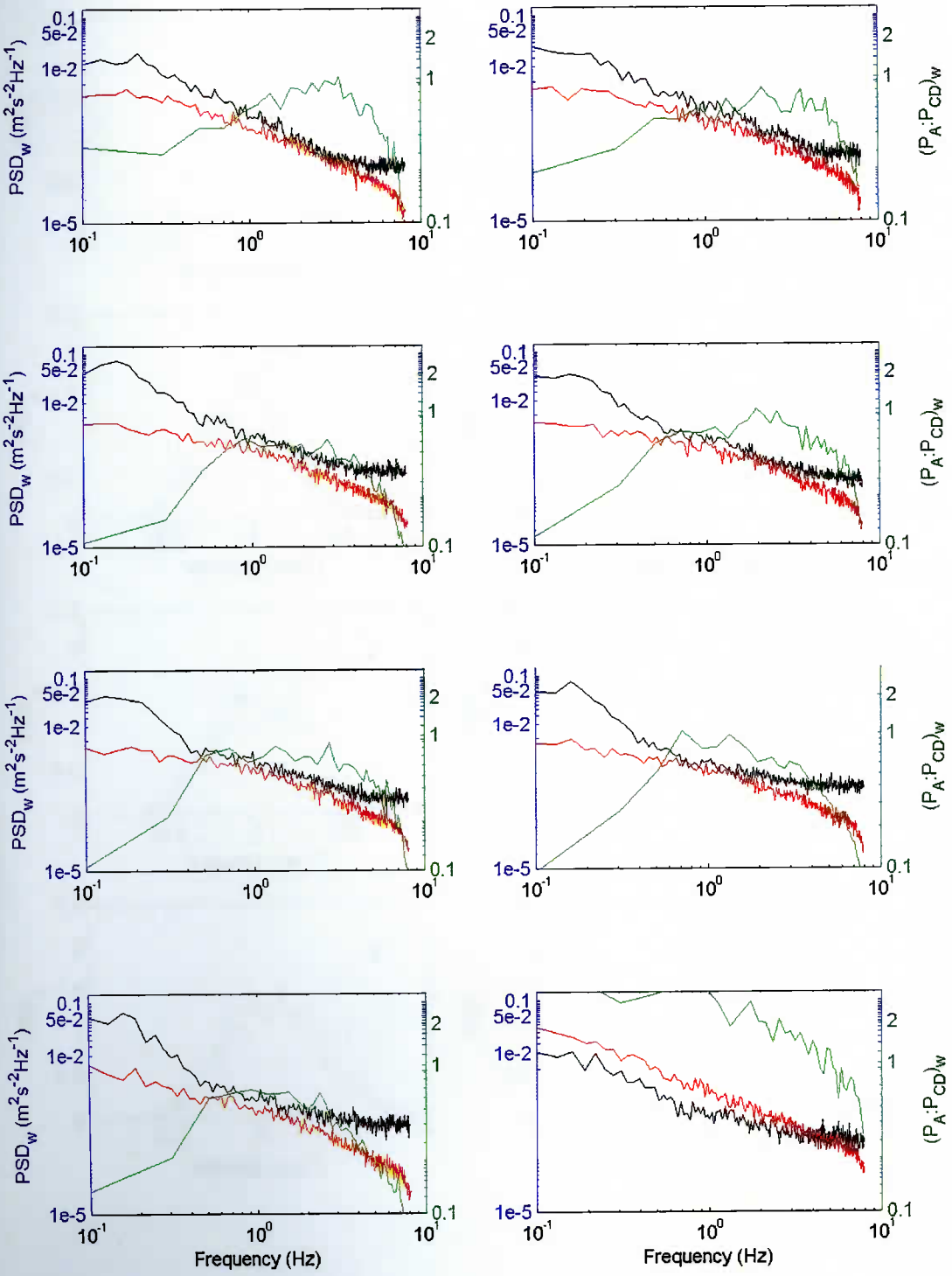

Figure 21. The power spectra of the zero-mean w velocities are plotted in red for the ADV_S and black for the CDVP; the ratio of the spectra is shown by the green plot, with the axis scale indicated on the right side of the figure.

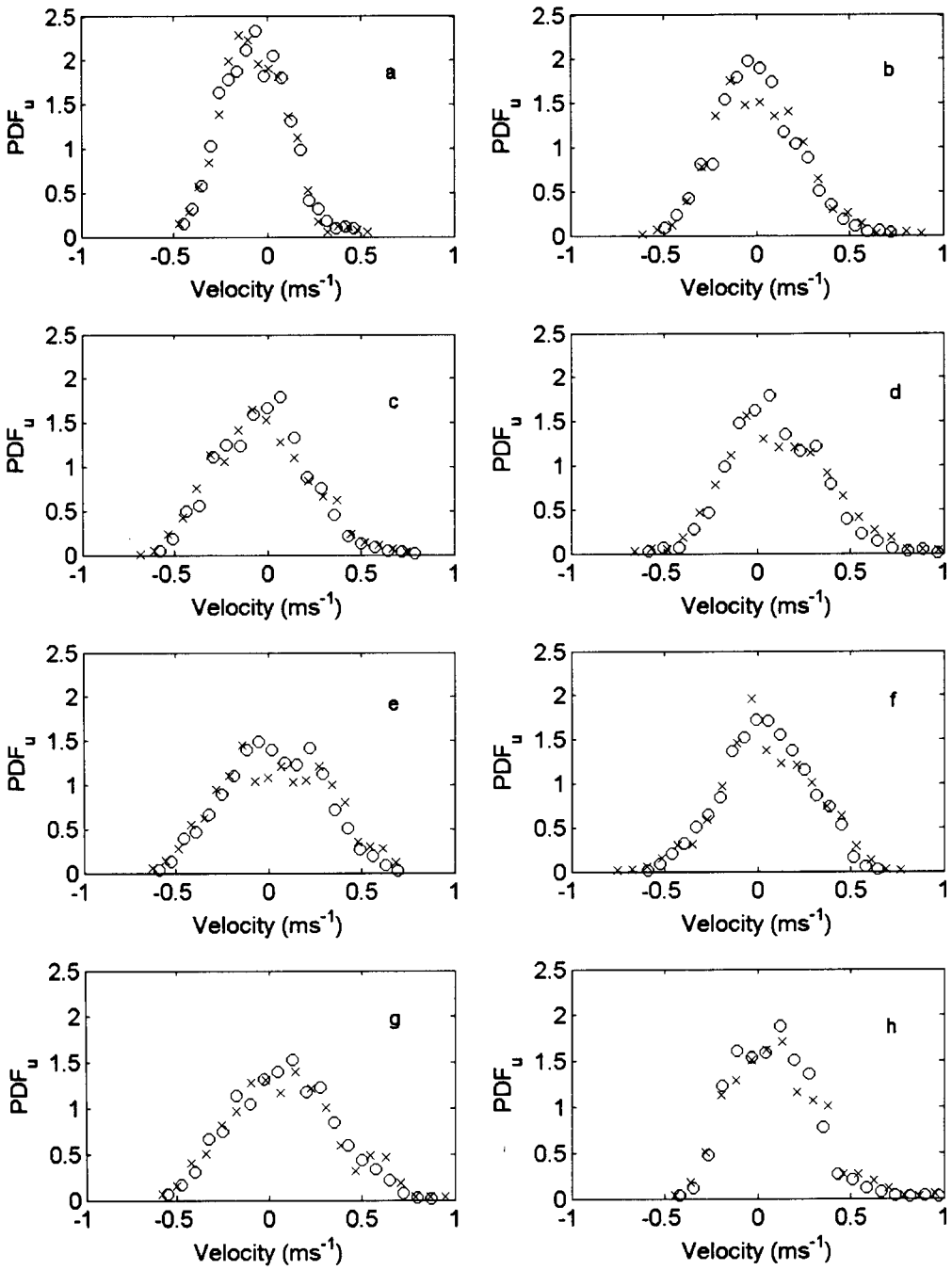

Figure 22 The probability density functions of the zero-mean velocities, u, are plotted for the ADV-S (o) and the CDVP (x).

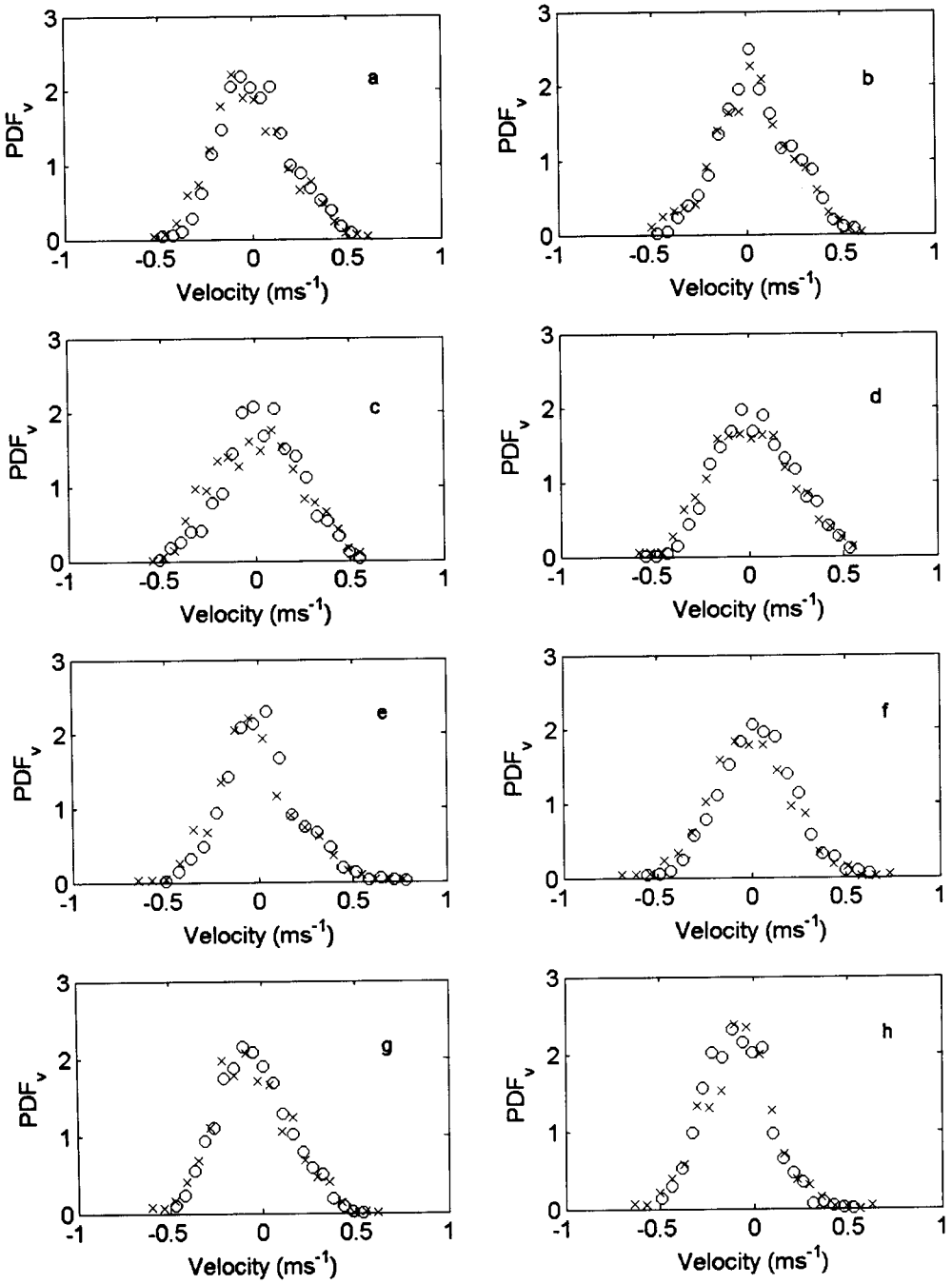

Figure 23 The probability density functions of the zero-mean velocities, v, are plotted for the ADV-S (o) and the CDVP (x).

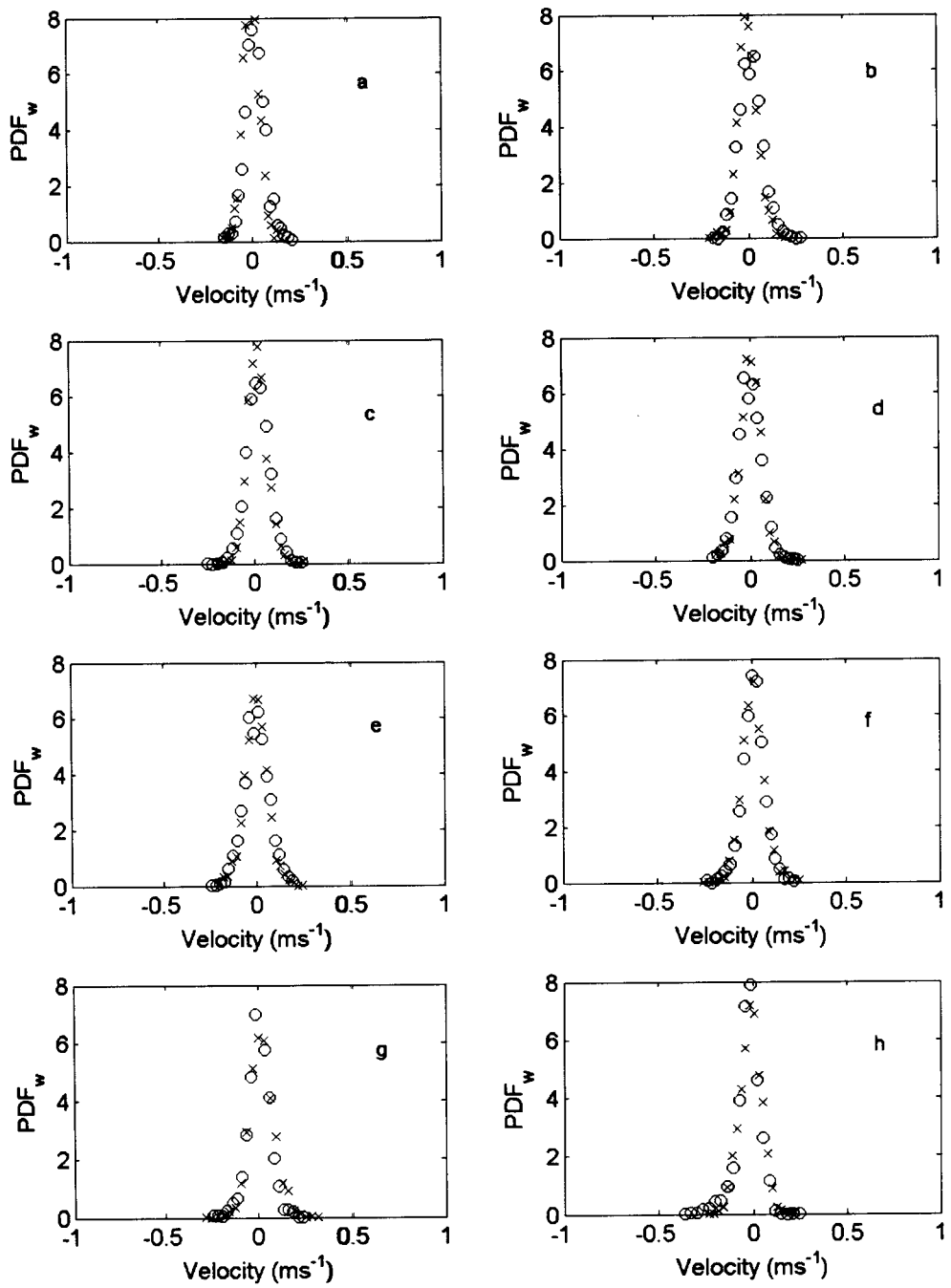

Figure 24 The probability density functions of the zero-mean velocities, w, are plotted for the ADV-S (o) and the CDVP (x).

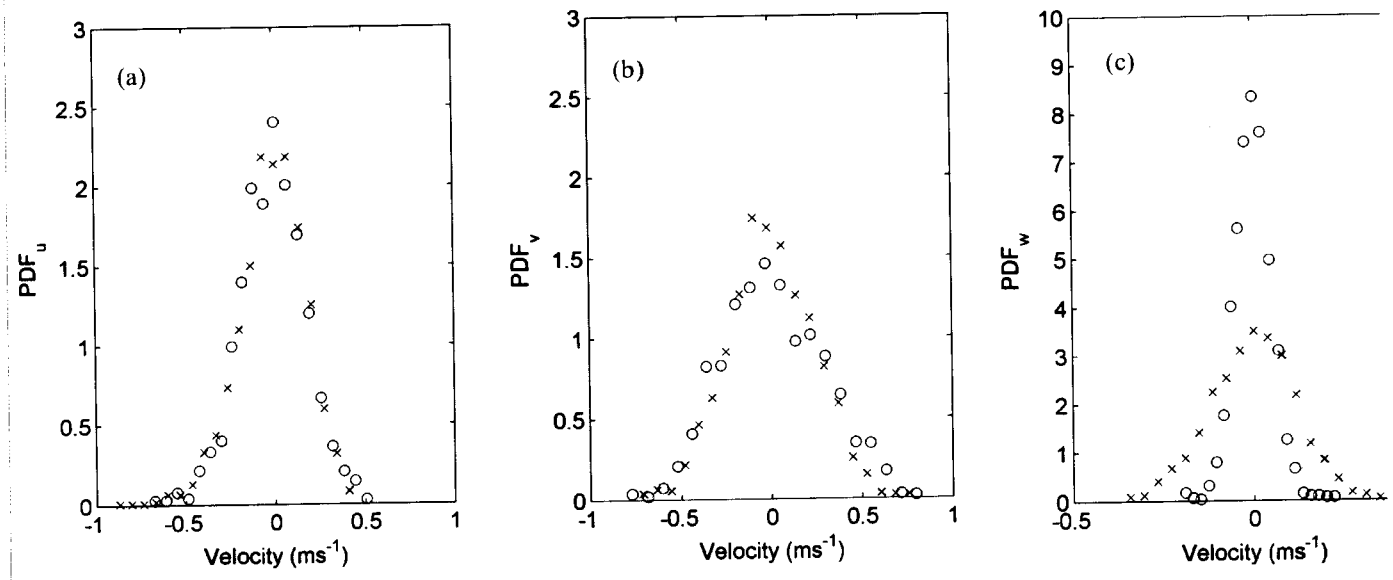

Figure 25 An example of the probability density functions of the zero-mean velocities, (a) u, (b) v, and (c) w plotted for the ADV-N (o) and the CDVP (x), from the 4th record of the flood tide.

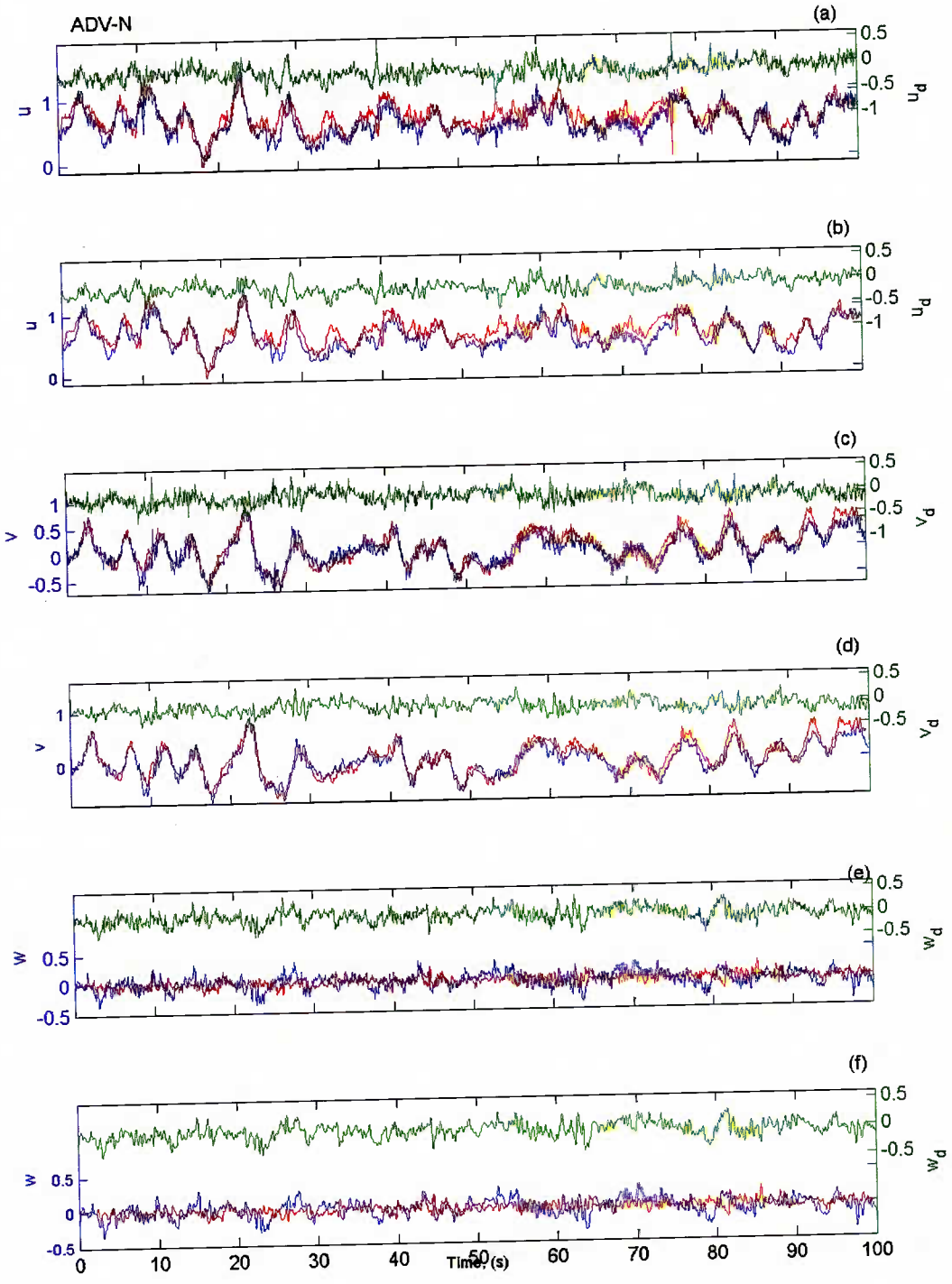

Figure 26 These time series plots show the ADV-N (red) and CDVP (blue) data at 16 Hz (a,c and e) and also after filtering with a 4 Hz cut-off for each component u, v and w. (b,d and f).

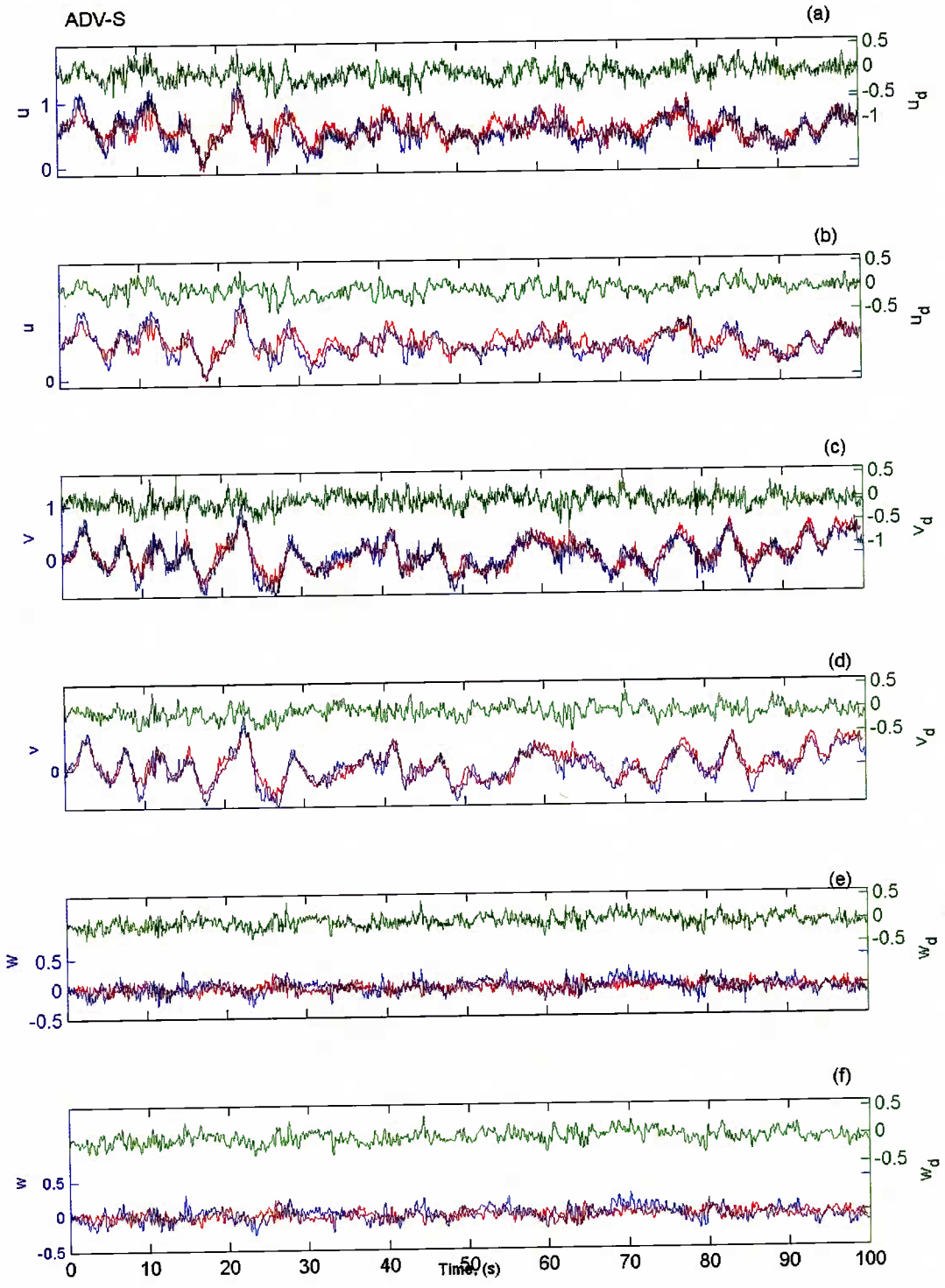

Figure 27 These time series plots show the ADV-N (red) and CDVP (blue) data at 16 Hz (a,c and e) and also after filtering with a 4 Hz cut-off for each component u, v and w. (b,d and f).

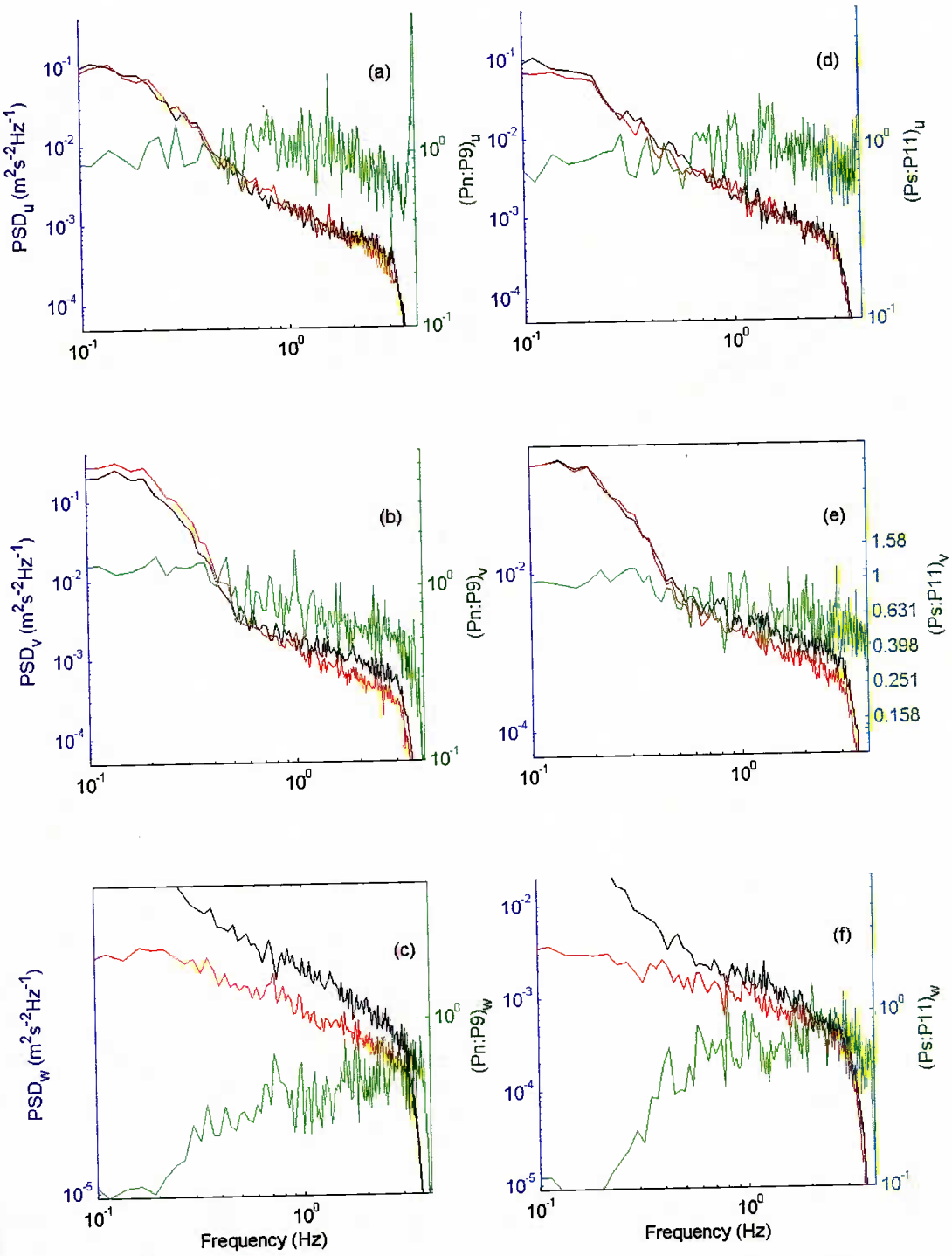

Figure 28 . The power spectra of the zero-mean filtered velocities for u,v and w at 11:29 are plotted in red for the ADV_N and black for the CDVP in figures a,b and c, and for the ADV_S in figures d,e and f; the ratio of the spectra is shown by the green plot, with the axis scale indicated on the right side of the figure.

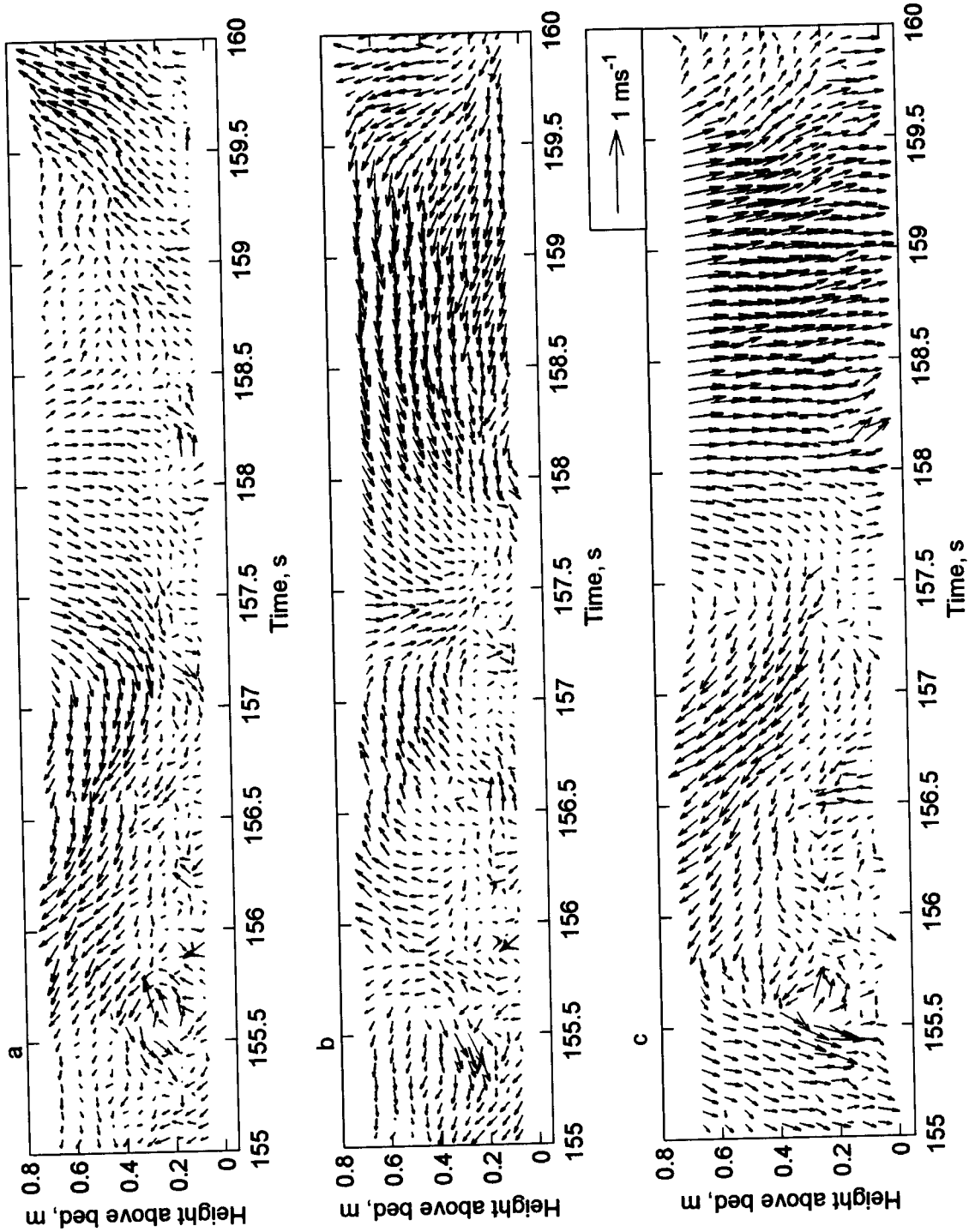

Figure 29 This plot demonstrates the capability of the triple axis CDVP to aid with the visualisation of the wave and turbulent flow. Plots (a) (b) and (c) show a time series over a 5 second period of the zero-mean velocities displayed as vectors uw, vw and uv. The vertical scale covers the range measured by the profiler in 0.05 m steps above the bed.